A tale of two gyres: Contrasting distributions of dissolved cobalt and iron in the Atlantic Ocean during an Atlantic Meridional Transect (AMT-19)

Rachel U. Shelley, Neil J. Wyatt, Glenn A. Tarran, Andrew P. Rees, Paul J. Worsfold, Maeve C. Lohan

▶ **To cite this version:**

Rachel U. Shelley, Neil J. Wyatt, Glenn A. Tarran, Andrew P. Rees, Paul J. Worsfold, et al.. A tale of two gyres: Contrasting distributions of dissolved cobalt and iron in the Atlantic Ocean during an Atlantic Meridional Transect (AMT-19). Progress in Oceanography, 2017, 158, pp.52-64. 10.1016/j.pocean.2016.10.013 . hal-01483143

HAL Id: hal-01483143
https://hal.science/hal-01483143

Submitted on 19 May 2020

HAL is a multi-disciplinary open access archive for the deposit and dissemination of scientific research documents, whether they are published or not. The documents may come from teaching and research institutions in France or abroad, or from public or private research centers.

L'archive ouverte pluridisciplinaire **HAL**, est destinée au dépôt et à la diffusion de documents scientifiques de niveau recherche, publiés ou non, émanant des établissements d'enseignement et de recherche français ou étrangers, des laboratoires publics ou privés.

A tale of two gyres: Contrasting distributions of dissolved cobalt and iron in the Atlantic Ocean during an Atlantic Meridional Transect (AMT-19)

R.U. Shelley, N.J. Wyatt, G.A. Tarran, A.P. Rees, P.J. Worsfold, M.C. Lohan

ABSTRACT

Cobalt (Co) and iron (Fe) are essential for phytoplankton nutrition, and as such constitute a vital link in the marine biological carbon pump. Atmospheric deposition is an important, and in some places the dominant, source of trace elements (TEs) to the global ocean. Dissolved cobalt (dCo) and iron (dFe) were determined along an Atlantic Meridional Transect (*AMT*-19; Oct/Nov 2009) between 50 °N and 40 °S in the upper 150 m in order to investigate the behaviour and distribution of these two essential, bioactive TEs. During *AMT*-19, large differences in the distributions of dCo and dFe were observed. In the North Atlantic gyre provinces, extremely low mixed layer dCo concentrations (23 ± 9 pM) were observed, which contrasts with the relatively high mixed layer dFe concentrations (up to 1.0 nM) coincident with the band of highest atmospheric deposition (~5-30 °N). In the South Atlantic gyre, the opposite trend was observed, with relatively high dCo (55 ± 18 pM) observed throughout the water column, but low dFe concentrations (0.29 ± 0.08 nM). Given that annual dust supply is an order of magnitude greater in the North than the South Atlantic, the dCo distribution was somewhat unexpected. However, the distribution of dCo shows similarities with the distribution of phosphate (PO_4^{3-}) in the euphotic zone of the Atlantic Ocean, where the North Atlantic gyre is characterised by chronically low PO_4, and higher concentrations are observed in the South Atlantic gyre (Mather et al., 2008), suggesting the potential for a similar biological control of dCo distributions. Inverse correlations between dCo and *Prochlorococcus* abundance in the North Atlantic gyre provinces, combined with extremely low dCo where nitrogen fixation rates were highest (~20-28° N), suggests the dominance of biological controls on dCo distributions. The contrasting dCo and dFe distributions in the North and South Atlantic gyres provides insights into the differences

between the dominant controls on the distribution of these two bioactive trace metals in the central Atlantic Ocean.

INTRODUCTION

Cobalt (Co), like iron (Fe), is essential for phytoplankton growth (e.g. Morel et al. 1994; Saito et al. 2002; Sunda and Huntsman, 1995a; 1995b; Timmermans et al. 2001; Rodriguez and Ho., 2015). Cobalt is the metal centre in the vitamin B_{12}.(cobalamin) complex which is essential for the synthesis of amino acids, deoxyriboses, and the reduction and transfer of single carbon fragments in many biochemical pathways. Cobalt is required for the de novo synthesis of vitamin B_{12} by marine prokaryotes (Bonnet et al. 2010). However, the majority of eukaryotic marine phytoplankton are B vitamin auxotrophs, acquiring their vitamin B_{12} requirements through a symbiotic relationship with bacteria (Croft et al., 2005; Cruz-Lopez and Maske, 2016), although this pathway might not be a simple linear flux from producer to consumer (Helliwell et al., 2016). Cobalt is also the metal co-factor in the metalloenzyme, carbonic anhydrase (CA), which is required for inorganic carbon acquisition by *Prochlorococcus*, and *Synechococcus* (Sunda and Huntsman, 1995a; Saito et al., 2002). In addition, *Trichodesmium* require Co for nitrogen fixation (Rodriguez and Ho, 2015), and Co can substitute for zinc (Zn) as the metal co-factor of the protein PhoA in the enzyme alkaline phosphatase (AP) (Gong et al., 2005; Sunda and Huntsman, 1995a). The production of AP facilitates acquisition of phosphorus (P) from the organic-P pool by phytoplankton and bacteria (e.g. Mahaffey et al., 2014). In addition, the strong correlation between dissolved Co (dCo) and inorganic-P (phosphate,PO_4) in the upper water column, across diverse oceanic regimes (Saito and Moffett, 2002; Noble et al., 2008; 2012; Bown et al., 2011; Dulaquais et al., 2014a; Baars and Croot, 2015), indicates the nutritive role of Co.

The role of iron (Fe) as an essential requirement for phytoplankton growth is well documented (e.g. Martin et al., 1990; Coale et al, 1996; Boyd et al., 2007). For example,

photosystems I and II are Fe intensive, and Fe is required for enzymatic process at nearly all stages of the microbial nitrogen cycle, including nitrogen fixation (Morel and Price, 2003; Küpper et al., 2008; Richier et al., 2012). Despite Fe being the fourth most abundant element in the Earth's crust, dissolved Fe (dFe) is often only present at trace concentrations (< 0.5 nM) in oxygenated surface waters of the open ocean (Blain et al., 2008; Measures et al., 2008; Ussher et al., 2013). Consequently, primary production is limited by low Fe-availability in 30 - 40% of the world's oceans (Moore et al, 2002; Boyd and Ellwood, 2010). In the Atlantic Ocean, a number of studies have demonstrated that primary production can be under Fe-stress or limitation, seasonally in association with the spring bloom. (Moore et al., 2006; Nielsdottir et al., 2009), as well as in regions where subsurface nutrient supply is enhanced (Moore et al., 2013, and references therein). The supply of Aeolian Fe is also a key control on the distribution of diazotrophs (Mills et al., 2004; Moore et al., 2009). In addition to Fe, light, macronutrients (N, P, Si), vitamins (e.g. B_{12}) and micronutrients (e.g. Co, Zn) may also (co-)limit marine productivity (Bertrand et al., 2007; Saito et al., 2008; Moore et al., 2013; Browning et al., 2014).

A major vector of trace elements (TEs) to Atlantic surface waters is atmospheric deposition (Jickells et al., 2005; Baker et al., 2006; 2007; Sarthou et al., 2007; Buck et al., 2010; Evangelista et al., 2010; Ussher et al., 2013; Shelley et al., 2015), much of which originates from Northwest Africa (Prospero and Carlton, 1972). An estimated 240 ± 80 Tg of dust is transported westwards annually (Kaufman et al., 2005), primarily during the summer months. Approximately 40% of annual global dust deposition occurs in the North Atlantic Ocean (Jickells et al., 2005); the majority of this into waters beneath the Saharan dust plume (~ 5 - 30° N) (Mahowald et al., 1999; Prospero et al., 2002; Kaufman et al., 2005). Hence, it is between these latitudes that surface Fe concentrations are highest (Measures et al., 2008; Fitzsimmons et al., 2013; Ussher et al., 2013). Wet deposition in the Intertropical Convergence Zone (ITCZ) scavenges aerosols from the atmosphere, effectively preventing the southwards transport of North African aerosols (Schlosser et al.,

2013). Thus the seasonal migration of the ITCZ drives the latitudinal gradient in aerosol dust loading (Prospero and Carlson, 1972; Doherty et al., 2012: 2014; Tsamalis et al., 2013), and hence surface water Fe concentrations and results in a concomitant shift in the latitudinal distribution of diazotrophy and corresponding dissolved inorganic-P depletion (Schlosser et al., 2013). Despite Co being less abundant in crustal material than Fe (Fe 3.9%, Co 0.002%; Rudnick and Gao, 2003), atmospheric deposition is a source of Co to surface waters. (Shelley et al., 2012; Dulaquais et al., 2014a). Consequently, we anticipated that Co concentrations would also be highest under the Saharan plume due to the sheer volume of dust that is deposited.

Another important source of trace metals to remote Atlantic surface waters is through vertical mixing. This mechanism reportedly provides ~ 5-35 % of the dFe input flux to the Atlantic mixed layer (Ussher et al., 2013). Vertical mixing is particularly important in the tropics where elevated sub-surface dFe concentrations are associated with low oxygen, upwelled water (Bergquist and Boyle, 2006; Measures et al., 2008; Fitzsimmons et al., 2013; Ussher et al., 2013). On the other hand, lateral advection of Fe from shelf regions to the remote Atlantic Ocean is reported to range from minimal (Laes et al., 2007; Ussher et al., 2007; Noble et al., 2012; Fitzsimmons et al., 2013) to significant in the vicinity of 20 °N (Rijkenberg et al. (2012). For Co, understanding the contribution of these sources is hindered by a relative paucity of data. However, lateral transport has recently been reported in both the eastern and western basins of the Atlantic (Noble et al., 2012; Dulaquais et al., 2014a; 2014b).

Iron and Co distributions are also strongly influenced by both redox speciation and organic complexation. Although Fe^{2+} is the more bioavailable form of Fe (Shaked and Lis, 2012), the thermodynamically favoured species of Fe in oxic seawater (pH 8) is Fe^{3+}. However, Fe^{3+} is relatively insoluble under these conditions, and is rapidly scavenged from the water column and forms insoluble Fe^{3+} oxyhydroxides (Liu and Millero, 2002). Chelation by organic ligands increases the solubility of Fe in seawater; both strong (e.g.

siderophores) and weaker ligand classes (e.g., humics) have been shown to be play a role in maintaining Fe in solution (Mawji et al., 2008; Croot and Heller, 2012; Heller et al., 2013; Buck et al., 2015). Similarly, Co^{2+} in also thermodynamically favoured in oxic seawater, and Co forms strong organic complexes (Ellwood and van den Berg, 2001; Saito and Moffett, 2001; Baars and Croot, 2015).

The primary removal mechanism for Co and Fe from the euphotic zone is through biological uptake (Martin and Gordon, 1988; Moffett and Ho, 1996). In addition, adsorptive scavenging on to particles (Moffett and Ho, 1996; Johnson et al., 1997; Wu et al., 2001; Bruland and Lohan, 2003) and aggregation and sinking (Croot et al., 2004) are also important removal pathways for both Co and Fe.

The Atlantic Meridional Transect (*AMT*) programme provides an ideal platform to investigate Co and Fe cycling in the upper Atlantic Ocean and the role of these metals on climate-relevant biological processes. Here we report the geographical distribution and biogeochemistry of Co and Fe in the upper water column along a 12,000 km, gyre-centred transect of the Atlantic Ocean (*AMT-19*) between ~ 50° N and 40° S. As our knowledge of Fe biogeochemistry is arguably more advanced than for Co, the following discussion aims to develop our understanding of Co biogeochemistry in the upper water column (≤ 150 m) of the Atlantic Ocean between 50° N and 40 °S by making comparisons with dissolved Fe distributions from this and earlier studies.

MATERIALS AND METHODS

Sampling

Twenty nine stations were sampled during cruise *AMT-19* (13/10/09–28/11/09) from Falmouth, UK to Punta Arenas, Chile, on board the *R.R.S. James Cook* (Fig. 1). Stations were sampled from the six biogeographical provinces listed in Figure 1, described by Longhurst (1998). In this study, the distribution of salinity, temperature, dCo, dFe and

macronutrients (nitrate and phosphate) were used to identify the province boundaries (Table 1). The assigned province boundaries are subject to small-scale variations due to their seasonal drift, as is the ITCZ, a region that forms the boundary between the atmospheric hemispheres which migrates seasonally from a position centred at ~5°N in boreal winter to ~10°N in the boreal summer (Sultan and Janicot, 2000).

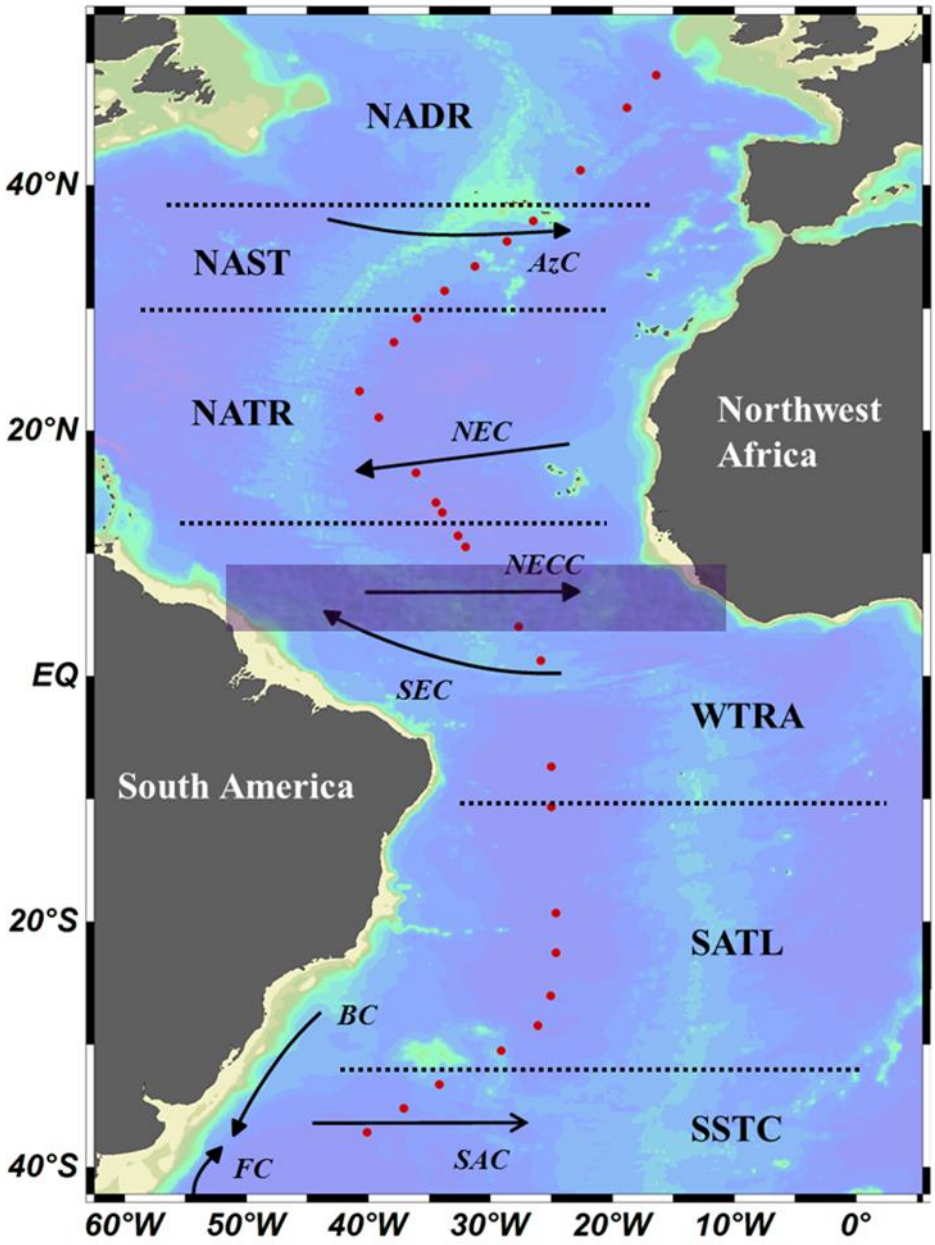

Figure 1. AMT-19 cruise track, showing the 29 water column stations and the biogeochemical provinces (Longhurst, 1998) defined in this study: North Atlantic Drift (NADR,38-56°N), North Atlantic Gyre (NAST,30-38°N), North Atlantic Tropical Gyre (NATR,12-30°N), Western Tropical Atlantic (WTRA,12°N-10°S), South Atlantic Gyre (SATL,10-33°S), and South Atlantic Subtropical Convergence (SSTC, 33-55°S), and Atlantic Ocean surface currents: AzC = Azores Current, NEC = North Equatorial Current, NECC = North Atlantic Counter Current, SEC = South Equatorial Current, BC = Brazil Current, SAC = South Atlantic Current, FC = Falklands Current. The approximate position of the ITCZ (4-9°N with the most intense rain activity between 4-5°N) during November 2009 was identified from the Giovanni data product (http://giovanni.sci.gsfc. nasa.gov), and is marked by the shaded box.

Samples for the determination of dCo and dFe were collected from 10 L trace metal-clean Teflon coated Ocean Test Equipment (OTE) bottles, attached to a titanium CTD rosette. Samples for macronutrients were collected from ten depths during each titanium CTD rosette deployment to correspond with trace metal sampling, and additionally from standard 20 L Niskin bottles fitted to a stainless steel CTD rosette (Seabird), thus providing high resolution profiling along the cruise track. All ship-based trace metal sample handling was conducted in a pressurised clean van. Seawater samples for dCo and dFe were filtered into acid-cleaned, low density polyethylene (LDPE) bottles (Nalgene) using a 0.2 µm Sartobran 300 filter capsule (Sartorius) and acidified to pH 1.7-1.8 (0.024 M) with ultraclean hydrochloric acid (HCl, Romil SpA) inside a class-100 laminar flow hood. Samples for the determination of TdFe were not filtered prior to acidification to 0.024 M HCl. All samples were then double zip-lock bagged for storage prior to analysis in the home laboratory.

Dissolved cobalt determination

Dissolved Co was determined in the ISO accredited clean room facility (ISO 9001) at Plymouth University, UK by flow injection with chemiluminescence detection (FI-CL; Shelley et al., 2010). Briefly, the flow injection manifold was coupled with a photomultiplier tube (Hamamatsu, model H 6240-01). The dCo was determined in UV-irradiated samples (3 h;

400 W medium-pressure Hg lamp, Photochemical Reactors) from the chemiluminescence produced from the catalytic oxidation of pyrogallol (1,2,3-trihydroxybenzene), the chemiluminescence emission was recorded using LabVIEW v.7.1 software. Due to the extremely stable nature of organic complexes of Co in seawater, several studies have demonstrated the requirement to UV irradiate samples prior to analysis in order to liberate strongly-complexed Co (Vega and van den Berg, 1997; Donat and Bruland, 1988; Saito et al., 2005; Shelley et al., 2010). During all analytical runs UV-irradiated SAFe D2 reference samples were analysed (n = 4; measured value, 50 ± 2 pM; consensus value 46± 3 pM). Typically, blank values were 4 ± 1 pM (n = 8), with a detection limit of 3 pM (blank + 3σ).

Dissolved and total dissolvable iron determination

Dissolved Fe and total dissolvable Fe (TdFe; unfiltered seawater) were also determined using FI-CL in the same clean room facility as the dCo. The Fe FI-CL method used in this study was based on the method originally described by Obata et al. (1993) and modified by de Baar et al. (2008). Briefly, measurements were made based on the catalytic oxidation of luminol (5-amino-2,3-dihydrophthalazine-1,4-dione; Aldrich) by hydrogen peroxide (H_2O_2) in the presence of Fe. As this method detects Fe(III), this study used a H_2O_2 oxidation step whereby H_2O_2 (10 nM) was added to each sample 1 h prior to the determination of Fe(III) (Lohan et al., 2005). Chemiluminescence emission was detected by a Hamamatsu photomultiplier tube (model H 6240-01) and recorded using LabVIEW v.7.1 software. The accuracy of the method was assessed for every analytical run by the determination of dFe in SAFe S and D1 seawater reference materials. The concentrations of dFe measured in the SAFe reference samples were in good agreement with the consensus values (measured value, S = 0.12 ± 0.04 nM, n = 13; D1 = 0.72 ± 0.08 n = 14; consensus value, S = 0.093 ± 0.008 nM; D1 = 0.67 ± 0.04).

192 Consensus values for dCo and dFe were reported to the GEOTRACES
193 Intercalibration Committee in 2010 (dCo) and 2011 (dFe), and are available
194 at:http://geotraces.org/science/intercalibration/322-standards-and-reference-materials.

195

196 *Nutrients, temperature, salinity and chlorophyll-a*

197 Dissolved inorganic macronutrients, phosphate (PO_4^{3-}) and nitrate (NO_2^- + NO_3^- = Σ
198 NO_3) were analysed on-board within 3-4 h of collection using a 5-channel segmented flow
199 autoanalyser (Bran and Luebbe, AAII AutoAnalyzer) following standard colorimetric
200 procedures (Grashoff et al. 1983) modified by Woodward et al. (1999). Low-level nutrients
201 were not determined using liquid wave guides during *AMT*-19.

202 Salinity, temperature and dissolved O_2 were measured using a CTD system (Seabird
203 911+). Dissolved O_2 was determined by a Seabird SBE 43 O_2 sensor. Salinity was calibrated
204 on-board using discrete samples taken from the OTE bottles using an Autosal 8400B
205 salinometer (Guildline), whilst dissolved O_2 was calibrated using an automated photometric
206 Winkler titration system (Carritt and Carpenter, 1966). Chlorophyll fluorescence and beam
207 attenuation were determined using an Aquatraka MkIII fluorometer and Alphatraka MkII
208 transmissometer (Chelsea Instruments), respectively. Sampling depths were determined by
209 reference to the *in situ* fluorescence, temperature, salinity and irradiance (photosynthetically
210 active radiation, PAR, 400–700 nm) profiles, to include 97%, 55%, 33%, 14%, 1% and 0.1%
211 PAR levels. For chlorophyll-*a* determination, samples were filtered (0.2 µm polycarbonate)
212 and the filters extracted in 10 mL of 90 % acetone overnight at 4° C (Welschmeyer et al.,
213 1994). The chlorophyll-*a* extract was measured on a pre-calibrated (pure chlorophyll-*a*
214 standard, Sigma-Aldrich) Turner Designs Trilogy 700 fluorimeter.

215 *Prochlorococcus* and *Synechococcus* were enumerated by flow cytometry using a
216 Becton Dickinson FACSort (Oxford, UK) flow cytometer equipped with an air-cooled laser
217 providing blue light at 488 nm (Tarran et al. 2006).

218 The trace metal (dCo, dFe and TdFe) data, ancillary data and a full station list are available
219 at: http://www.bodc.ac. uk/ projects/uk/amt/

220

221 RESULTS

222 *Hydrographic setting and macronutrient distributions*

223 The six biogeographical provinces used in this study are shown in Figure 1. Note that
224 the North Atlantic gyre is divided into two separate provinces; the North Atlantic subtropical
225 gyre (NAST) and the North Atlantic tropical gyre (NATR). In these provinces, the
226 thermohaline structure of the upper water column (Fig. 2) is primarily determined by the
227 water masses that occupy each region and the relative evaporation and precipitation rates.
228 In the North Atlantic, the lowest upper water column temperatures (12-22°C) were observed
229 in the NADR. Here, the water column displayed weak thermohaline stratification,
230 characteristic of high wind stress in the NADR during boreal autumn (Longhurst, 1998).

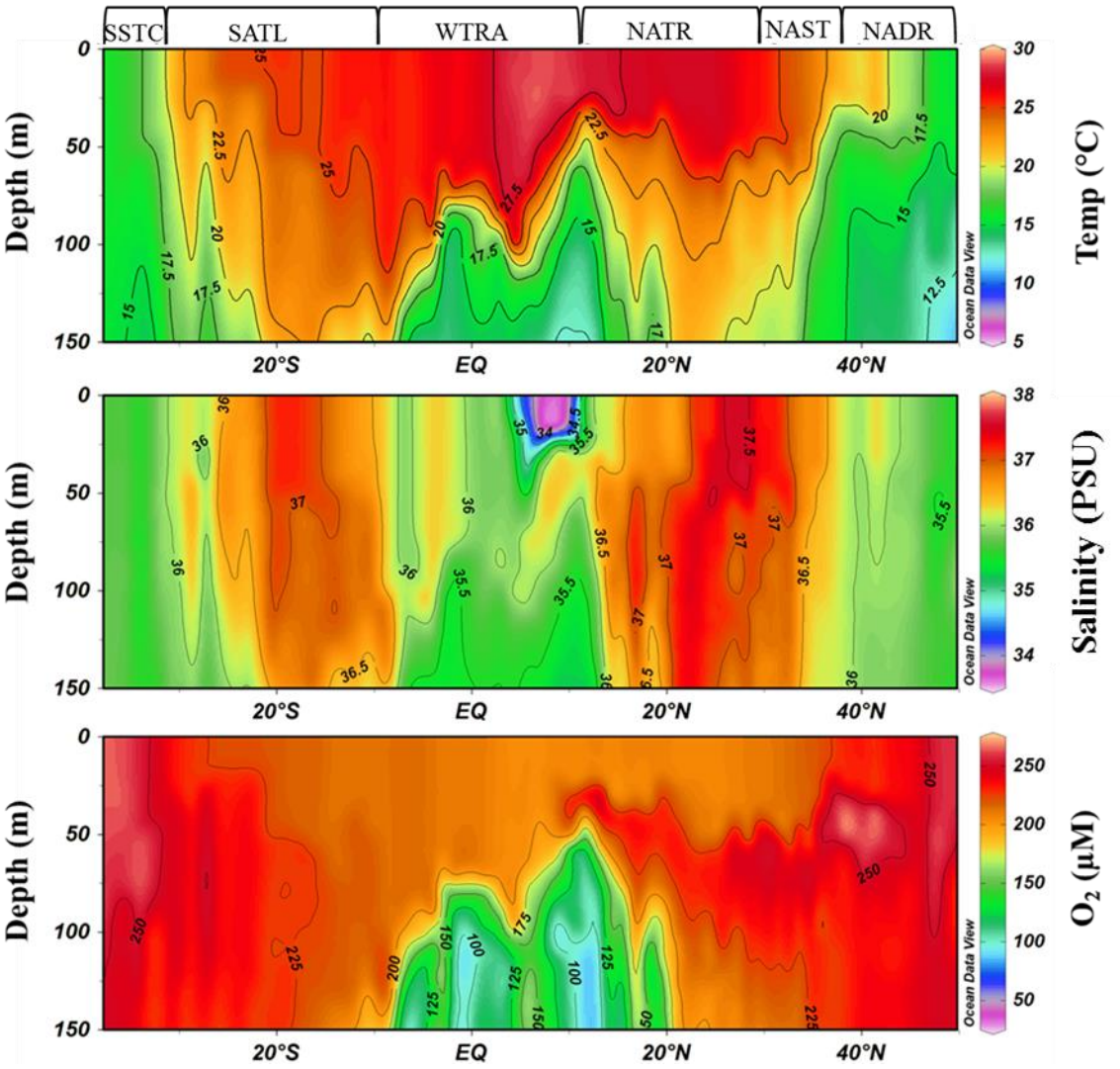

Figure 2. The distributions of temperature (top), salinity (middle) and dissolved oxygen (bottom) in the upper 150 m of the Atlantic Ocean during *AMT*-19, with the biogeochemical provinces marked above (refer to Figure 1 for acronyms). Stations were sampled approximately every 1-1.5° of latitude at a 1 m depth resolution.

In the NAST, the introduction of warmer (> 20° C), more saline (> 36.5), water from the Gulf Stream enters via the Azores Current (AC, centred at 35-36 °N) (Aiken et al., 2000) resulting in a mixed layer depth of between 40 and 50 m. Further south in the NATR, the North Equatorial Current (NEC, centred at 15 °N) supplies water with salinity > 37, due to the high rates of evaporation at these latitudes. Consistent with previous *AMT* observations (Aiken et al., 2000; Robinson et al., 2006), the NEC was observed to depths of ~ 150 m between 20 and 26° N during *AMT*-19.

Towards the southern extent of the NATR province, a plume of cooler (< 20° C), fresher (< 36), lower oxygen (< 150 µM) upwelled water was clearly visible below 60 m (Fig. 2). This oxygen minimum zone (OMZ), which extended throughout the tropical Atlantic to the southern boundary of the WTRA, results from the divergence between the North Equatorial Current (NEC) and the North Equatorial Counter Current (NECC) at ~ 10° N, and the divergence between the NECC and the South Equatorial Current (SEC) at ~ 2° S (Hastenrath and Merle, 1987; Longhurst, 1998; Aiken et al., 2000) (Fig. 1). Mixed layer depths (defined as the depth at which potential density differed by 0.05 kg m^{-3} from the surface) in the WTRA varied between 9 and 95 m. Throughout the upper 150 m of the WTRA low salinity (< 36.5) water, relative to the sub-tropical gyres, was observed caused by dilution through excess precipitation over evaporation (Aiken et al., 2000).

A surface salinity minimum (< 35) was observed in the WTRA between ~6 and 10° N to a depth of 30 m (Fig. 2), a common feature that can arise from either converging air masses and subsequent high precipitation rates in the ITCZ, or from Amazon Water transported eastwards across the Atlantic by the NECC (Aiken et al., 2000). However, no elevation in surface silicate concentration (data not shown), which would be indicative of Amazon Water, was observed during *AMT*-19. In addition, two intense rainfall events were recorded between 6 and 9 °N during the cruise, suggesting that the high rates of precipitation that characterise the ITCZ could be the cause of the WTRA salinity minimum.

As observed during earlier *AMT* studies (Robinson et al., 2006), a gradual latitudinal decrease in sea surface temperature and salinity was observed in the SATL (10-33° S) and into the SSTC (33 -38° S), a manifestation of the decrease in evaporation rates associated with lower temperatures at higher latitudes. An increase in the westerly winds as the ship travelled south, coupled with increased downwelling associated with the anti-cyclonic circulation of the sub-tropical gyre (Longhurst, 1998; Ussher et al., 2013), resulted in a deepening of the SATL mixed surface layer down to 61 m, and a fully homogeneous upper water column (T ~ 16 °C, S ~ 35.5) in the SSTC.

The distribution of macronutrients along the transect (Fig. 3; NO_3 data is not shown due to the similarity with the distribution of PO_4) revealed extremely low mixed layer concentrations (PO_4 < 0.05 µM) in the NAST and NATR and three distinct regions where concentrations below the mixed layer were elevated. Firstly, in the NADR, macronutrient concentrations were elevated below 60 m (PO_4 = 0.2-0.9 µM, NO_3 = 2.5-12 µM). These elevated concentrations continued into the northern section of the NAST before becoming depleted. Secondly, macronutrient concentrations were elevated in waters associated with the equatorial upwelling (PO_4 =0.2-1.5 µM, NO_3 = 2.5- 23 µM). Thirdly, macronutrient concentrations in the SSTC were elevated below 100 m (PO_4 = 0.2- 0.5 µM; NO_3 = 2.5- 5 µM), values similar to those reported for the Southwest Atlantic at 40° S by Wyatt et al. (2014).

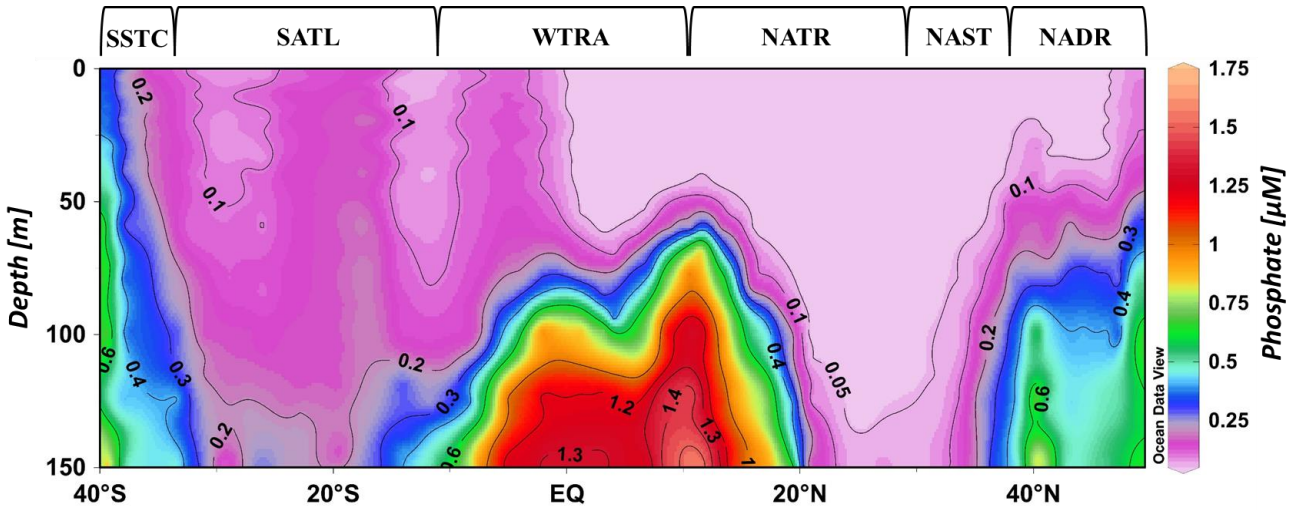

Figure 3. Distribution of phosphate (PO_4) in the upper 150 m of the Atlantic Ocean during *AMT* 19 with the biogeochemical provinces marked above (refer to Figure 1 for acronyms). Note the higher concentrations in the SATL compared to the NAST and NATR.

Dissolved Co and Fe distributions

Surface water (upper 25 m) dCo and dFe distributions during *AMT*-19 displayed distinct differences between the North and South Atlantic (Fig. 4). Surface dCo concentrations during *AMT*-19 were highly variable (10-93 pM). The lowest concentrations were observed in the northern gyre provinces (NAST 25 ± 14 pM and NATR 21 ± 2.8 pM, respectively, n = 6),

whilst higher concentrations were observed in the upwelling region (WTRA 51 ± 38 pM, n = 9) and the South Atlantic gyre (SATL 60 ± 31 pM, n = 3) (Fig. 4) This trend is similar to that previously reported for PO_4, with very low concentrations of PO_4 (0.01-0.05 µM) observed in the North Atlantic gyre regions and higher concentrations (0.2-0.5 µM) in the South Atlantic gyre (Mather *et al.,* 2008). At approximately 28° S the SATL is sub-divided into two cells separated by the subtropical counter-current. To the south of this front (25-30° S) the Brazil Current (BC) forms the southern extent of a recirculation cell (Mémery et al. 2000 and references therein). The high surface dCo in this region (89 ± 4 pM at 28.8°S, 26.1°W, Fig. 4) is attributed to offshore advection of continental Co mobilised by the western boundary current and a declining gradient is observed to the south of this frontal region.

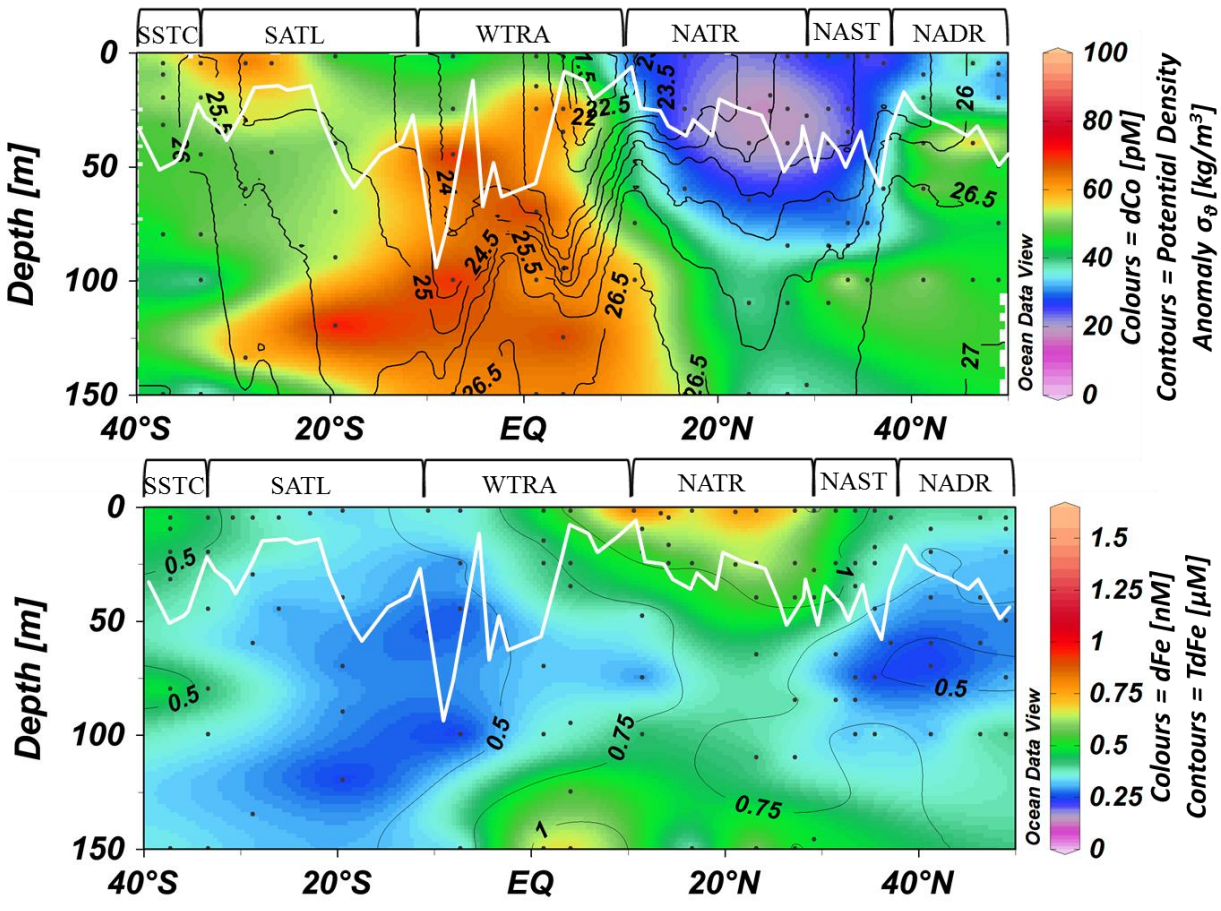

Figure 4. The distribution of dCo (pM) overlaid with potential density anomaly (kg m^{-3}; top panel), dFe (nM) overlaid with the TdFe (nM; bottom panel) in the upper 150 m of the Atlantic Ocean during *AMT*-19, with the approximate depth of the mixed layer marked (MLD) shown as a solid white line. The biogeochemical provinces are displayed above the top panel (refer to Figure 1 for acronyms).

The surface water (upper 25 m) dFe and TdFe distribution is in complete contrast to dCo, as dFe and TdFe were relatively high in the NATR and NAST, and low in the SATL (Fig. 4). The highest surface dFe and TdFe concentrations were observed in the NATR (dFe, 0.68 ± 0.28 nM; TdFe, 1.1 ± 0.25 nM, n = 12 and 10, respectively) and the WTRA (dFe, 0.76 ± 0.61 nM; TdFe 1.3 ± 0.33 nM, n = 6) provinces between ~ 5 and 30° N, corresponding to the latitudinal extent of the Saharan plume (5-30° N) (Prospero et al. 2002; Kaufman et al., 2005). Here, two distinct surface dFe maxima were observed. The first, located between ~ 20 and 28° N (dFe, 0.88 ± 0.14 nM, n = 6), was in the vicinity of the elevated rates of surface nitrogen fixation (0.85-1.1 nmol L^{-1} d^{-1}) determined during this study (data not shown, but available from www.bodc.ac.uk). The second, at ~10-14° N (0.74 ± 0.58 nM, n = 7), overlapped with the ITCZ surface salinity minimum (Fig. 2), which is consistent with the observation that high rainfall rates associated with the ITCZ contributes to high wet deposition fluxes of Fe in the south NATR/north WTRA (Kim and Church, 2002; Powell et al., 2015). The locations of these two surface dFe maxima coincided with high TdFe concentrations (1.1 ± 0.17 nM and 1.3 ± 0.28 nM, respectively) between 4 – 30° N, and are in excellent agreement with observations from previous North Atlantic studies (Bowie et al., 2002; Bergquist and Boyle, 2006; Measures et al., 2008; Ussher et al., 2013). Combined with the low dFe in the SATL, the peaks in dFe and TdFe in the North Atlantic gyre provinces indicate the importance of atmospheric deposition in controlling surface dFe concentrations (e.g., Schlosser et al. 2013). North of ~ 30° N, surface dFe concentrations were lower (0.34 ± 0.14 nM, n = 14) and less variable (Fig. 4), most likely due to a reduced Saharan dust input and strong winter mixing in the NAST and NADR, compared with weak seasonal mixing in the NATR (Longhurst, 1998).

In sub-surface waters (deeper than 25 m), the dCo distribution was also a tale of sharp contrasts. Extremely low concentrations were observed throughout the North Atlantic gyre provinces, with the lowest concentrations (16 ± 3.4 pM, n = 8) observed at the base of the mixed layer. The maximum abundances of *Prochlorococcus* (> 4 x 10^5 cells mL^{-1}), a

335 cyanobacteria with an absolute requirement for Co (Sunda and Huntsman, 1995a), in the
336 North Atlantic gyre provinces were observed in the southern NATR in concert with a shoaling
337 of the MLD, and were accompanied by very low dCo concentrations (13-17 pM at 35-40 m
338 depth), suggesting biological drawdown as an important control of dCo distribution in this
339 region. Higher dCo concentrations were observed in the provinces adjoining the northern
340 gyre provinces, e.g., in the NADR (dCo = 59 ± 23 pM, n = 10) *Prochlorococcus* were less
341 abundant and dCo appears to be advected southwards along the 26 kg m^{-3} isopycnal (Fig. 4,
342 top panel) to ~ 40°N and the boundary with the NAST.

343 The highest sub-surface dCo concentrations (e.g. 89 ± 4 pM at 28.8°S, 26.1°W) were
344 observed in the SATL. Between 25-150 m, the SATL was characterised by relatively high
345 dCo (52 ± 15 pM, n = 10), and decreasing temperature and salinity with increasing latitude.
346 At the dynamic SATL/SSTC boundary (33.3°S, 34.2°W), a slight increase in dCo was
347 observed at 80 m relative to the surrounding water (58 pM at 80 m, 44 pM at 45 m and 29
348 pM at 100 m). The source of this high dCo is not immediately clear, but may result from spin-
349 off of eddies containing higher dCo water from the south. The presence of eddies in this
350 region is confirmed by the sea surface anomaly image, Fig. S1 in the Supplementary
351 Material. As concentrations of dCo can be highly variable over scales of ~10 km (Saito and
352 Moffett, 2002; Noble et al. 2008; Shelley et al. 2012), the low dCo observed at the adjoining
353 station (15.5 ± 0.3 pM at 35.3°S, 37.1°W) may be just as characteristic of this province
354 (reflecting seawater that has had no contact with the continental shelf and low atmospheric
355 inputs) as water with high dCo. Regardless of the dCo concentration, in all gyre provinces
356 dCo exhibited a broadly nutrient-type distribution (lower concentrations in the mixed layer
357 than below it) in the upper 150 m.

358 The sub-surface distribution of dFe also displayed strong latitudinal gradients (Fig. 4.) In a
359 reversal of the trend for dCo, sub-surface dFe concentrations in the SATL were low and
360 relatively uniform (0.26 ± 0.06 nM, n = 12) compared with the northern gyre provinces (0.40
361 ± 0.17 nM, n = 25) where atmospheric deposition is much higher. Below 100 m in the

northern NATR/southern NAST waters between 23 and 31° N, the dFe and TdFe concentrations were 0.48 ± 0.14 nM (n = 5) and 0.72 ± 0.11 nM (n = 5), respectively and could be a relic of a previous atmospheric deposition event. Interestingly, we observed a similar feature at the same depth for dCo (36 ± 3.4 pM; Fig. 4).

For both dCo and dFe, elevated sub-surface concentrations were associated with the low oxygen waters. Maximum sub-surface dCo and dFe concentrations (62 ± 16 pM and 0.62 ± 0.20 nM, respectively) were observed between 0-10 °N, coincident with an oxygen minimum of 100 -150 µM (Fig. 2). Observations of elevated dFe in this OMZ are consistent with previous studies (Bergquist and Boyle, 2006; Measures et al., 2008; Fitzsimmons et al., 2013; Ussher et al., 2013) suggesting that the elevated dFe may be a steady-state feature in this region, sustained by either remineralisation of high Fe:C organic matter formed in the Fe-rich surface and/or lateral mixing of high dFe water from sedimentary sources. However, in contrast to dFe, the elevated dCo concentrations were not confined to the OMZ, but extended over a broader latitudinal range (southwards) and wider depth range, suggesting that mechanisms other than remineralisation and low dissolved oxygen concentrations were sustaining the elevated dCo concentrations in this region.

DISCUSSION

Given that there are a number of similarities in the redox and organic speciation of Co and Fe, the difference in the distributions of these two elements in the Atlantic Ocean is stark. In the northern gyre provinces (NATR and NAST), where deposition and dissolution of atmospheric aerosols is the dominant source of Fe (e.g. Duce and Tindale, 1991; Duce et al. 1991; Sarthou et al., 2003; Jickells et al., 2005; Baker et al., 2006; Buck et al., 2010; Evangelista et al., 2010; Ussher et al., 2013), the extremely low concentrations of dCo contrast strongly with the relatively high concentrations of dFe. A number of studies have alluded to an atmospheric source of Co which could influence surface dCo concentrations in

388 regions of high atmospheric deposition (Bowie et al. 2002; Dulaquais et al., 2014a; Knauer
389 et al, 1982; Thuroczy et al., 2010; Wong et al. 1995). Furthermore, aerosol Co is significantly
390 more soluble than aerosol Fe (Dulaquais et al., 2014a; Mackey et al., 2015; e.g. 8-10%
391 fractional solubility for Co and 0.44-1.1% fractional solubility for Fe for the same Saharan
392 dust samples, Shelley et al., 2012), further supporting the assertion that atmospheric supply
393 may play a pivotal role in controlling surface distributions of dCo and hence influence
394 phytoplankton community dynamics.

395 For dFe, the sharpest gradient was observed at the NAST/NATR boundary, and is
396 almost certainly linked to atmospheric inputs and the approximate location of the northern
397 extent of the Saharan plume. Indeed the relationship between dFe in the upper water
398 column and atmospheric supply are well documented (e.g. Bowie et al., 2002; Baker et al.
399 2006, 2007; 2013; Rijkenberg et al., 2012; Ussher et al., 2013), which makes the low dCo in
400 the same latitudinal band somewhat of a paradox. One explanation could be that the Co is
401 being scavenged in the water column following oxidation by manganese (Mn) oxidising
402 bacteria, which oxidise both Mn and Co via a common microbial pathway (Moffet and Ho,
403 2001). However, significant removal via the Mn co-oxidation pathway is not supported by the
404 literature in open ocean environments, as it is driven by competitive inhibition (Moffett and
405 Ho, 1996; Noble et al., 2012) and dCo is low (this study; A. Noble, pers. comm.) and dMn is
406 high (Wu et al., 2014; Hatta et al., 2015) in the northern gyre provinces.

407 In the vicinity of the ITCZ, both dFe and TdFe were significantly inversely related to
408 salinity in the mixed layer (r^2 = 0.89 and 0.82 respectively; $p < 0.05$, n = 5) suggesting that
409 the scavenging of dust incursions into the ITCZ (Adams et al., 2012) as it migrated south
410 towards to its boreal winter position (centred at ~ 5° N) could be a source of Fe to surface
411 waters at the NATR/WTRA border, as described by Kim and Church (2002). However, the
412 small number of samples (n = 5) make any links tenuous at best, particularly as this
413 relationship is driven by the high dFe and TdFe values (both 1.1 nM) at 1.5 m depth at 10.6
414 °N, 32.0 °W. Similarly, the relatively sparse dCo dataset for mixed layer waters influenced by

the ITCZ (n = 4) makes assessing a link between dCo and precipitation unrealistic, and is further complicated by the limited literature on dCo in rainwater of the ITCZ and the contrasting conclusions reached; i.e. either precipitation dilutes surface dCo (Helmer and Schremms, 1995; Pohl et al., 2010), or it is a source of dCo (Bowie et al., 2002). In this study, two modest enrichments of dCo (relative to the underlying water and to adjoining stations) coincided with rain events at ~ 31 °N, and the intense rain events in the ITCZ at 6 and 9 °N (M. Chieze, pers. Comm; www.giovanni. sci.gsfc.nasa.gov). At 31 °N, for example, the concentration of dCo was 46.4 pM at 2 m depth, whereas at 25 m depth dCo had been drawn down to 21.2 pM. In addition, wet deposition has been estimated to account for >90% of the total atmospheric deposition flux of Co, compared with just 20% for Fe, based on data from Bermuda (T. Church, unpublished data). In the eastern tropical Atlantic (in September-November), Powell et al. (2015) estimate that wet deposition may be a relatively more important source of Fe than in the western North Atlantic gyre, contributing up to 70% of the total atmospheric flux.

We have estimated the soluble Co and Fe deposition fluxes for 20 °N and 20 °S from dry deposition data published in Shelley et al. (2015) and Dulaquais et al. (2014a) (20 °N) and Chance et al. (2015) (20 °S) (Table 1). For Co, in the NATR, under the Saharan outflow, dry deposition contributes only 1.4% of the mixed layer depth (MLD) concentration of dCo (assuming permanent stratification of the water column). In contrast, atmospheric deposition may supply twice the amount of dFe observed in the mixed layer over the course of the year. In the SATL, where atmospheric deposition may be orders of magnitude lower, atmospheric supply alone cannot account for the concentrations of either metal observed (<<0.5% and 21% of mixed layer dCo and dFe, respectively). It is noted that these atmospheric deposition fluxes do not account for wet deposition, and thus, the estimates presented in Table 1 may be rather conservative. Nonetheless, these data highlight the role of atmospheric deposition in controlling the dFe concentrations in surface waters of the two gyre regions. For Co, the impact of atmospheric deposition is more subtle.

Our calculations are sensitive to the percentage of the metal that is soluble in seawater. Unfortunately, aerosol metal solubility is poorly constrained. In Table 1, a Co solubility value of 9.0% is used for the NATR (Dulaquais et al., 2014a). However, Co solubility is a function of the composition of the bulk aerosol, which in turn is a function of aerosol provenance, and may be up to threefold higher (i.e., ~30%, R. Shelley, unpublished data, available at: www.bco-dmo.org) in aerosols sourced from Europe as opposed to those from North Africa, due to a higher component of industrial emission aerosols in the former. This will result in a higher flux of soluble Co, and given the extremely low concentrations of dCo in the northern gyre provinces, suggests that atmospheric supply may still have an important role in supplying Co to surface waters (Thuroczy et al., 2010).

Table 1. Estimation of the contribution of atmospheric dry deposition to the mixed layer (ML) inventories of dCo and dFe. The values used are from: a = Shelley et al. (2015); b = Dulaquais et al., 2014a; c= this study; d = Chance et al. (2015), respectively.

Metal	Location	Dry depo. flux	Solubility	Soluble flux		MLD	MLD [dCo, dFe]	Annual accumulation in ML
		μg m^{-2} d^{-1}	%	μg m^{-2} d^{-1}	nM m^{-2} d^{-1}	m	nM	nM
Cobalt	20 N	1.6 (a)	9.0 (b)	0.14 (a, b)	24 (a, b)	40 (c)	16.2 (c)	0.22
Cobalt	~ 20 S	0.0029 (d)	2.0 (d)	0.000058 (d)	0.010 (d)	45 (b)	37 (b)	0.000080
Iron	20 N	3600 (a)	0.31 (a)	11.2 (a)	201 (a)	40 (c)	0.90 (c)	1.80
Iron	~ 20 S	3.2 (d)	2.9 (d)	0.093 (d)	1.7 (d)	45 (c)	0.33 (c)	0.014

If, as our data suggests, aerosols are indeed a source of Co to the northern gyre provinces, how can the contrasting distributions of dCo and dFe be reconciled? We hypothesise that biological uptake primarily by the dominant components of the bacterial assemblage, such as the cyanobacteria *Prochlorococcus* and *Trichodesmium,* is exceeding supply, leading to a dCo deficit in the northern gyre provinces (NAST, NATR).

Biological controls on dissolved Co distributions

Although *Prochlorococcus* are ubiquitous in tropical and sub-tropical oceans, their range extends throughout the Atlantic from ~50 °N – 40 °S (Heywood et al., 2006). *Prochlorococcus* thrive in oligotrophic conditions and have an obligate requirement for Co for carbon fixation (Sunda and Huntsman, 1995a; Saito et al., 2002). During *AMT*-19, *Prochlorococcus* dominated the picoplankton assemblage, with *Synechococcus* only proliferating where *Prochlorococcus* abundance was less than 10^5 cells mL^{-1} (Fig. 5), i.e., the temperate margins of this *AMT* transect (NADR and SSTC), and in the low-salinity (<35) surface waters of the ITCZ (upper 30 m at 6-10 °N; Fig.2). Our data are consistent with the observation that *Prochlorococcus* typically outnumber *Synechococcus* by one to two orders of magnitude in stratified, oligotrophic waters (Durand et al., 2001).

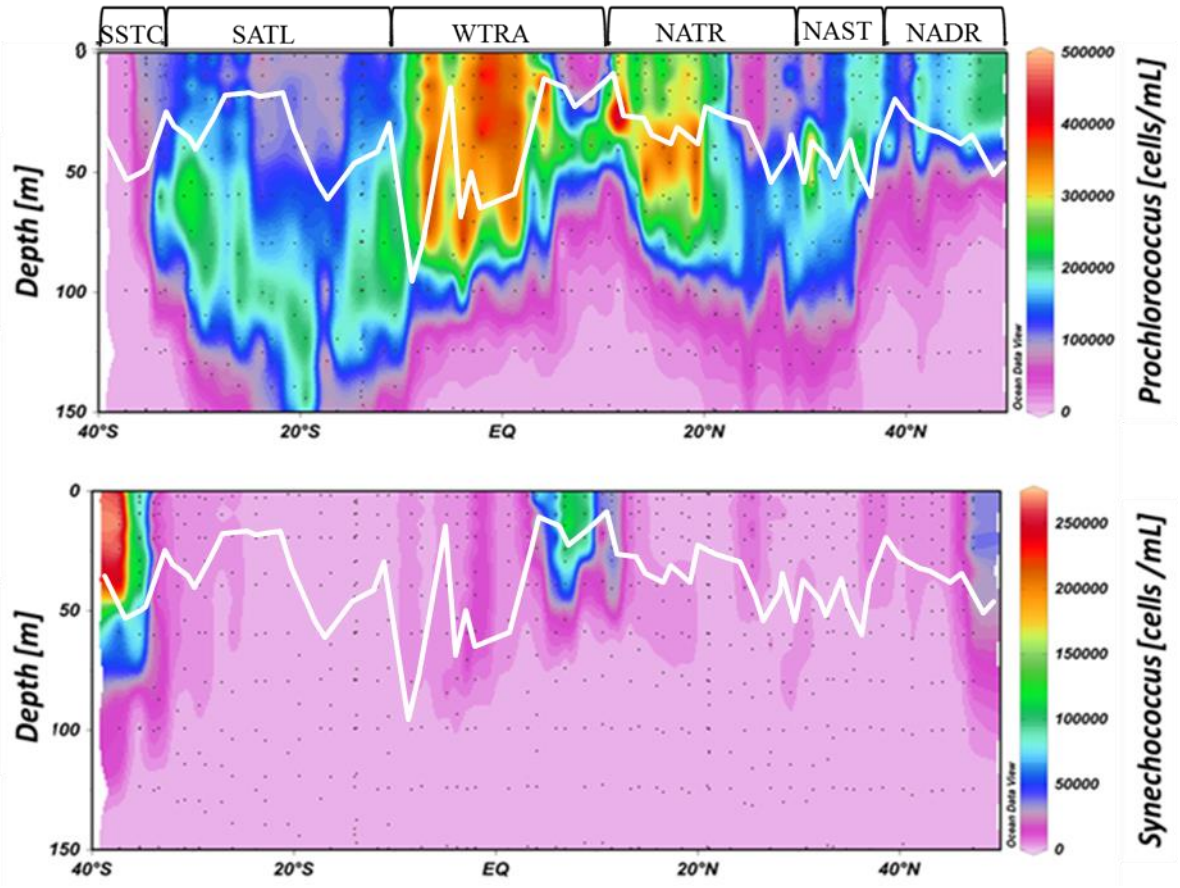

Figure 5. *Prochlorococcus* and *Synechococcus* distributions in the upper 150 m during *AMT*-19. The white line depicts the approximate depth of the mixed layer.

476 In this study, the highest abundances of *Prochlorococcus* were observed in the high-
477 dCo tropical upwelling region (~5 °N-5 °S) (Fig. 5). This contrasts with the phytoplankton
478 dynamics in another high dCo upwelling region, the Costa Rica upwelling dome (CRD),
479 where *Synechococcus* dominated the picoplankton assemblage (Ahlgren et al., 2014).

480 In terms of *Prochlorococcus* abundance, the northern gyre was divided in two (at
481 approximately the boundary between the NATR and NAST). The NAST and NATR, were
482 both characterised by extremely low dCo concentrations, with the dCo minima (NAST = 15 ±
483 3.8, NATR = 15 ± 1.4 pM, at 28-45 m) generally corresponding with the maximum
484 abundances of *Prochlorococcus* in these provinces (Fig. 5). The *Prochlorococcus* maxima
485 were at shallower depths than the DCM (e.g., 4 x10^5 cells mL^{-1} at 29 m at 11.5 °N, compared
486 to a DCM of 0.41 µg L^{-1} chl-*a* between 46-50 m). The relationship between dCo
487 distributions, *Prochlorococcus* abundance, and the relative position of the DCM has
488 previously been observed in the Sargasso Sea (western NAST/NATR; Shelley et al., 2012).

489 In the NATR, *Prochlorococcus* abundance was high (>3x10^5 cells mL^{-1}), even though
490 dCo was extremely low (22 ± 15 pM). In the NAST, dCo was similarly low (22 ± 3.8 pM), but
491 *Prochlorococcus* abundance was lower than in the NATR (generally <2x10^5 cells mL^{-1}). As
492 atmospheric deposition decreases northwards from the NATR to NAST, we hypothesise that
493 aerosol supply indirectly impacts *Prochlorococcus* abundance via its role as a key source of
494 Co and Fe. Moreover, the sub-surface dCo minimum coincides with the region of maximum
495 rates of nitrogen fixation during *AMT*-19 (21 – 23°N), consistent with a Co requirement for
496 nitrogen fixation by *Trichodesmium* (Rodriguez and Ho, 2015), which are abundant in the
497 tropical to subtropical North Atlantic, but almost entirely absent between 5 and 30° S (Tyrrell
498 et al., 2003; Schlosser et al., 2013). In the SATL, dCo concentrations and *Prochlorococcus*
499 abundance were decoupled to the extent that the opposite trend was observed, with high
500 dCo and high abundances of *Prochlorococcus* occurring together. This occurred in concert
501 with a near absence of *Trichodesmium*, suggesting that the presence/absence of
502 *Trichodesmium* may also have an important role in driving the dCo distribution.

503 Moreover, the presence/absence of other bacteria may influence dCo distributions.
504 Although the bacterial abundance was roughly equivalent in the SATL and NATR/NAST
505 during *AMT*-19 (M. Zubkov, pers. comm.) differences in the bacterial community composition
506 have been reported between the two gyres (Schattenhofer et al., 2009; Friedline et al.,
507 2012). In addition to the cyanobacteria, the marine bacteria SAR11, require Co for vitamin
508 B_{12} (Carini et al., 2013) and are more abundant in the northern gyre provinces and WTRA
509 compared to the SATL (Schattenhofer et al., 2009; 2011; Friedline et al., 2012). Recent work
510 has demonstrated that bacteria are the first to directly respond to Saharan dust inputs of
511 trace elements and nutrients, and these authors argue that the bacterial assemblage is a key
512 mediator of trace metal distributions following dust deposition (Westrich et al., 2016). Thus,
513 the differences in bacterial community composition can impact the biogeochemical cycle of
514 Co and hence explain the differing dCo distributions between the northern and southern
515 gyres.

516 In addition to active uptake, *Trichodesmium*, which are abundant in the subtropical/
517 tropical North Atlantic due to the delivery of atmospheric Fe (Richier et al., 2012) and P
518 (Ridame et al., 2003), can scavenge both Fe (Rubin et al., 2011) and P from solution
519 (Sañudo-Wilhelmy et al., 2001). Could the same removal mechanism be an important sink
520 for Co? Although we do not have particulate Co or TdCo data for *AMT*-19, TdCo was
521 determined in surface samples (7 m depth) on *AMT*-3 (a similarly grye-centred AMT; Bowie
522 et al., 2002), where low concentrations of ~ 30 pM dCo (*AMT*-19) and TdCo (*AMT*-3) were
523 observed between 3 and 17 °N. In addition, recent studies of particulate Co in the Atlantic
524 Ocean, demonstrated that it was ~ 5% the concentration of dCo in a full-depth transect along
525 ~12 °S (Noble et al., 2012) and 12 ± 12 in the West Atlantic (Dulaquais et al., 2014a),
526 suggesting that scavenging may only be a minor sink for Co under a range of open ocean
527 environmental conditions.

528 Lastly, dCo distributions can be influenced by dissolved organic phosphorus (DOP)
529 acquisition. The region where extremely low dCo was observed is also where chronically low

PO_4 concentrations are observed (Mather et al., 2008). In the North Atlantic gyre provinces the DOP pool is 5-10 times higher than inorganic phosphorus and phytoplankton and bacteria must utilise AP to acquire their essential phosphorus requirement (Mahaffey et al., 2014). Zinc is the metal co-factor in the protein PhoA used for AP activity and, while Co can substitute for Zn as the metal centre in PhoA (Sunda and Huntsman 1995a), the preference is for Zn (Saito and Goepfert 2008). A recent study in the sub-tropical Atlantic has demonstrated that Zn concentrations, which are very low in this region, could limit AP activity (Mahaffey et al., 2014). Therefore, the low Co concentrations may arise from uptake by cyanobacteria and also from its substitution for Zn in AP. Using Co uptake results from freshwater phytoplankton grown under PO_4 limitation, Ji and Sherrell (2008) hypothesised, that the very high demand for Co in the tropical North Atlantic may be the result of persistent PO_4 stress in this region. However, the discovery of a calcium (Ca)-based AP (Kathuria and Martiny, 2011) suggests that at least some *Prochlorococcus* ecotypes and bacteria are able to bypass the need for Co in AP, which may reduce the potential for Co-Zn-P co-limitation. However, field based evidence in this region clearly shows that the AP activity is limited by Zn (Mahaffey et al. 2014) as a result of the extremely low dZn concentrations in the North Atlantic (Conway and John, 2014; Roshan and Wu, 2015) and with the low dCo concentrations observed in this study AP activity may also be limited by Co

In the SATL, *Trichodesmium* is largely absent (Tyrrell et al., 2003; Schlosser et al., 2013), and *Procholorococcus* abundance was lower, with maximum abundances deeper than in the northern gyre provinces likely due to significantly lower dFe concentrations, and a deeper MLD in the northern section of the SATL compared with the NATR/NAST (Figs. 4 and 5). The positive correlations between dCo and *Prochlorococcus* abundance in the South Atlantic (Fig. S2, Supplemental Material) may be linked with higher inorganic phosphorus availability, as well as higher dCo. In the South Atlantic, where atmospheric deposition is low, a combination of highly efficient internal cycling (85% of the dCo uptake rate in the SATL may be accounted for by remineralisation of organic matter, Dulaquais et al., 2014a),

lateral inputs (Bown et al., 2011; Noble et al., 2012) and relatively low biological demand results in higher dCo concentrations compared with the northern gyre provinces.

The different relationship between dCo and bacterial dynamics in the northern gyres and the SATL suggests that dCo availability has the potential to influence both the bacterial and phytoplankton community structure, or vice versa, through a complex interplay with other factors, such as Fe and inorganic phosphorus availability. However, the northern gyre provinces appear unique in the sense that biotic removal dominates and controls dCo distributions (Moffett and Ho, 1986). In future decades increased stratification and predicted increases in nitrogen supply (Behera et al., 2013) could exacerbate the disparity between the northern and southern gyres in terms of trace metal distributions as a result of proximal nutrient limitation and, thus, the potential for changes to the bacterioplankton community structure.

Low oxygen waters

Upwelling (vertical transport) can deliver macro- and micronutrient-enriched deep water to the mixed layer of the tropical North Atlantic, although for Fe the dominant flux is from the atmosphere (Ussher et al., 2013). Using the average dCo and dFe concentrations from below the surface mixed layer of the WTRA during *AMT*-19 (64 and 421 nmol m^{-3}, respectively) and an upward vertical mixing rate of 14.3 m y^{-1} (based on the method presented by Ussher et al., 2013 for a similar cruise track, *AMT*-16), we estimate an upward vertical mixing flux of 2.5 and 16.5 nM m^{-2} d^{-1} for dCo and dFe, respectively. The combination of this upward vertical transport of nutrient-rich water and atmospheric supply sustains relatively high algal biomass in surface waters of the tropical Atlantic (e.g., the maximum chl-*a* concentration of 0.41 µg L^{-1} was observed at 11.5 N at 46-50 m just above the thermocline and oxycline). These high levels of primary productivity result in a large amount of sinking detritus. Bacterial degradation of this detritus consumes oxygen which, in

turn, contributes to the development of OMZs. In the productive eastern equatorial Atlantic, a broad OMZ extends from ~100–900 m depth (Karstensen et al. 2008).

Both high dCo and dFe have previously been reported in the oxygen deficient waters of the WTRA (Bowie et al. 2002; Measures et al. 2008; Pohl et al. 2010) and during *AMT*-19 elevated dCo (> 60 pM) and dFe (> 0.60 nM) were observed in the OMZ of the WTRA. However, while elevated dFe in the sub-surface WTRA was associated with the OMZ (150 µM contour positioned at depths > 40–100 m depending on latitude), elevated sub-surface dCo covered a much wider depth range and was not confined to the WTRA, spilling over into the SATL at depths below ~ 100 m (Fig. 4). It is unlikely that the WTRA is supplying dCo to the SATL, as the two provinces are separated by the South Equatorial Current (SEC), and there is no evidence of elevated dFe to the south of the upwelling zone. Rather, preferential scavenging of Fe with respect to Co, in the Benguela and South Equatorial Currents (Noble et al., 2012), which feed into the South Atlantic gyre, provides the most likely explanation for the difference in dCo and dFe concentrations to the south of the upwelling zone.

During *AMT*-19, the 100 µM O_2 contour was observed to shoal to depths as shallow as 100 m, and in the WTRA as a whole the DCM was positioned just above the 150 µM O_2 horizon. In these productive waters bacterial degradation of sinking organic particles is evidenced by the apparent oxygen utilisation (AOU). Furthermore, the bacteria that consume the oxygen during the bacterial degradation of particles may be an additional source of high-affinity, metal binding ligands (Barbeau et al., 2001; 2003) which also retain remineralised Co and Fe in solution. While a positive relationship between dFe and AOU ($r^2 = 0.6$, $p = 0.03$, $n = 7$) in the latitudinal band 1-17 °N, was observed, for dCo and AOU the relationship was weak and not significant ($r^2 = 0.2$, $p = 0.3$, $n = 8$) (Fig. 6), suggesting that other sources of Co (e.g., vertical transport, lateral advection) are relatively more important in this region.

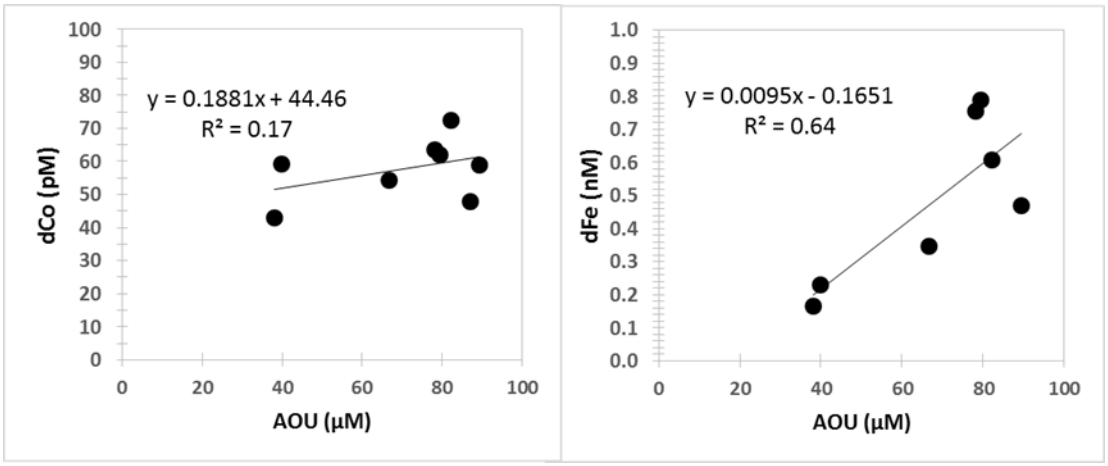

606

607 Figure 6. dCo (left) and dFe (right) plotted against the apparent oxygen utilisation (AOU; µM) in the
608 region of low dissolved oxygen (> 150 µM dissolved oxygen; 1-17 °N)

609

610 *Lateral transport*

611 In this study, surface dFe concentrations in the NADR of 0.20-0.58 nM were similar
612 to the 0.14-0.60 nM reported by Ussher et al. (2007) for Northeast Atlantic surface waters.
613 These authors observed a dFe concentration gradient over a relatively short distance
614 spanning the shelf break, and concluded that minimal lateral transport of dFe from the shelf
615 to the open ocean occurred in this region, despite severe winter storms. In this study, there
616 was little evidence for the lateral transport of dFe from the European shelf margin to the
617 open ocean. In contrast, in the NADR, a sharp gradient in dCo was observed at the
618 boundary with the NAST with the highest concentrations of dCo appearing to be transported
619 offshore along the 26.0 kg m^{-3} isopycnal. In the South Atlantic, although the
620 Falkland/Malvinas Current could potentially be a vector for the offshore transport of dFe,
621 here, too, we saw no evidence for the offshore transport of dFe

622 Lateral advection may however, be a more important source of dCo. Indeed, Bown et
623 al. (2011) report evidence of just such a mechanism in the Southeast Atlantic Ocean.
624 Furthermore, Noble et al. (2012) also observed a large-scale (> 2000 km), offshore dCo

plume in the SATL. These authors also noted offshore advection of dFe, but that the plume covered a far smaller distance (< 500 km) than the dCo plume, and despite no evidence for offshore advection of dMn (a tracer for sedimentary inputs), they concluded that reducing sediments on the African margin were a likely source of all three metals. However, dFe and dMn were scavenged preferentially to dCo, which explained the difference in the extent of the offshore plumes. Dulaquais et al. (2014b) also argue that scavenging is a fairly insignificant removal term for dCo in the western Atlantic, as they were unable to resolve dCo removal, via scavenging, from dilution by mixing.

To the south of the SATL, the cruise track passed through a dynamic frontal region, the confluence of the Brazil and the Falkland/Malvinas Currents. Both western boundary currents flow along the continental shelf until they meet and are deflected offshore. Indeed, Boebel et al. (1999) and Jullion et al. (2010) report cross frontal mixing in the Argentine Basin of the subtropical surface waters of the Brazil Current and sub-Antarctic Surface Water from the Southern Ocean at the Brazil- Falkland/Malvinas confluence. Furthermore, as only about 3% of fluvial Co is estimated to be retained within river systems (Sholkovitz and Copland, 1981), the northward flowing Falkland/Malvinas Current may also transport organically-complexed fluvial Co offshore, contributing to the elevated surface concentrations in this frontal region, as has previously been reported for Fe (Rijkenberg et al., 2014).

CONCLUSIONS

Dissolved Co and Fe distributions showed strong, and often contrasting, regional differences during *AMT*-19. Extremely low concentrations of dCo (NATR/NAST; ~20-30 pM) were observed in the northern gyre provinces where dFe was high, whereas the opposite trend was observed in the SATL. Both dCo and dFe distributions were generally nutrient-like; highlighting the nutritive role of these two bioactive elements. However, the extremely low

dCo of the northern gyre provinces is somewhat of a paradox given the seemingly plentiful supply of trace elements from Saharan dust. In these regions, we propose that dCo distribution in waters shallower than ~ 100 m is controlled predominantly by biological uptake by the bacteria (primarily *Prochlorococcus*, *Trichodesmium* and SAR11), and other organisms that utilise a Co analogue of AP for DOP uptake. This has important implications in the context of climate change, where stratification is predicted to increase, thus reducing phosphate inputs from below to surface waters. This situation may be further exacerbated by predicted increases in nitrogen deposition (Behera et al., 2013) as a result of increasing urbanisation/ industrialisation. Future studies should assess the potential for Co-Zn-P limitation in the North Atlantic.

ACKNOWLEDMENTS

With many thanks to the Captain and crew of RRS James Cook, and Carolyn Harris, Malcolm Woodward and Claire Widdicombe for kindly providing the nutrient, and the chl-*a* data, respectively. Thank you also to Mike Zubkov and Manuela Hartmann for discussion of bacterial abundance during AMT-19. We thank two anonymous reviewers for their valuable comments and suggestions. Funding for this work was provided through a Marine Institute (Plymouth University) Studentship to RUS, a Natural Environment Research Studentship (NERC) to NJW and NERC grant number NE/G016267/1 to MCL. Thank you also to the Atlantic Meridional Transect Programme co-ordinators who provided a berth on *AMT*-19 and therefore made this study possible. This study is a contribution to the international IMBER project and was supported by the UK NERC National Capability funding to Plymouth Marine Laboratory and the National Oceanography Centre, Southampton. This is contribution number 277 of the AMT programme.

REFERENCES

Adams, A.M., Prospero, J.M., and Zhang, C. 2012. CALIPSO-Derived Three-Dimensional Structure of Aerosol over the Atlantic Basin and Adjacent Continents. Journal of Climate 25: 6862-6879.

681 Aiken, J. et al. 2000. The Atlantic Meridional Transect: overview and synthesis of data.
682 Progress in Oceanography. 45: 257-312.

683 Baars, O., and Croot, P.L. 2015. Dissolved cobalt speciation and reactivity in the eastern
684 tropical North Atlantic. Marine Chemistry. 173: 310-319.

685 Baker, A. R., Jickells, T. D., Witt, M., and Linge, K. L. 2006. Trends in the solubility of iron,
686 aluminium, manganese and phosphorus in aerosol collected over the Atlantic Ocean. Marine
687 Chemistry. 98: 43-58.

688 Baker, A. R., Weston, K., Kelly, S. D., Voss, M., Streu, P., and Cape, J. N. 2007. Dry and
689 wet deposition of nutrients from the tropical Atlantic atmosphere: Links to primary
690 productivity and nitrogen fixation. Deep Sea Research Part I: Oceanographic Research
691 Papers. 54: 1704-1720.

692 Barbeau, K., Rue, E.L., Bruland, K.W. and Butler, A. 2001. Photochemical cycling of iron in
693 the surface ocean mediated by microbial iron(III)-binding ligands. Nature. 413: 409-413.

694 Barbeau, K., Rue, E.L., Trick, C.G., Bruland, K.W., and Butler, A. 2003. Photochemical
695 reactivity of siderophores produced by marine heterotrophic bacteria and cyanobacteria
696 based on characteristic Fe(III) binding groups. Limnology and Oceanography. 48: 1069-
697 1078.

698 Behera, S.N., Sharma, M., Aneja, V.P., and Balasubramanian, R., 2013. Ammonia in the
699 atmosphere: a review on emission sources, atmospheric chemistry and deposition on
700 terrestrial bodies. Environmental Science Pollution Research, 20, 8092-8131.

701 Bergquist, B. A., and Boyle, E.A. 2006. Dissolved iron in the tropical and subtropical Atlantic
702 Ocean. Global Biogeochemical Cycles. 20. Doi: 10.1029/2005GB002505.

703 Bertrand, E.M. et al. 2007. Vitamin B_{12} and iron co-limitation of phytoplankton growth in the
704 Ross Sea. Limnology and Oceanography. 52: 1079-1093.

Blain, S. et al. 2007. Effect of natural iron fertilisation on carbon sequestration in the Southern Ocean. Nature. 446: 1070-1074.

Boebel, O., Schmid, C., and Zenk, W. 1999. Kinematic elements of Antarctic Intermediate Water in the western South Atlantic. Deep Sea Research Part II. 46: 355-392.

Bonnet, S., Webb, E.A., Panzeca, C., Karl, D.M., Capone, D.G., and Sanudo-Wilhelmy, S.A., 2010. Vitamin B_{12} excretion by cultures of the marine cyanobacteria Crocosphaera and Synechococcus. Limnology and Oceanography, 55. Doi: 10.4319/lo.2010.55.5.1959.

Bowie, A.R., Whitworth, D. J., Achterberg, E. P., Mantoura, R. F. C., and Worsfold, P. J., 2002. Biogeochemistry of Fe and other trace elements (Al, Co, Ni) in the upper Atlantic Ocean. Deep Sea Research Part I: Oceanographic Research Papers. 49: 605-636.

Bown, J. et al., 2011. The biogeochemical cycle of dissolved cobalt in the Atlantic and the Southern Ocean south off the coast of South Africa. Marine Chemistry. 126: 193-206.

Boyd, P.W., and Ellwood, M.J. 2010. The biogeochemical cycle of iron in the ocean. Nature Geoscience. 3: 675-682.

Boyd, P. W. et al. 2007. Mesoscale iron enrichment experiments 1993-2005: synthesis and future directions. Science .315: 612-617.

Browning, T.J., Bouman, H.A., Moore, C.M., Schlosser, C., Tarran, G.A., Woodward, E.M.S., and Henderson, G.M., 2014. Nutrient regimes control phytoplankton ecophysiology in the South Atlantic. Biogeosciences, 11, 463-479.

Bruland, K. W. and Lohan, M.C. 2003. Controls of trace metals in seawater. In: The Oceans and Marine Geochemistry. Treatise on Geochemistry vol.6. (ed. H. Elderfield), pp 23-47. Oxford: Elsevier.

727 Buck, C. S., Landing, W.M., Resing, J.A. and Measures, C.I. 2010. The solubility and
728 deposition of aerosol Fe and other trace elements in the North Atlantic Ocean: Observations
729 from the A16N CLIVAR/CO_2 repeat hydrography section. Marine Chemistry. 120: 57-70.
730 Buck, K.N., Sohst, B., and Sedwick, P.N., 2015. The organic complexation of dissolved iron
731 along the U.S.GEOTRACES (GA03) North Atlantic Section. Deep Sea Research II, 116,
732 152-165.
733 Carini, P., Steindler, L., Beszteri, S., and Giovannoni, S.J. 2013. Nutrient requirements for
734 growth of the extreme oligotroph ‘Candidatus Pelagibacter ubique' HTCC1062 on a defined
735 medium. The ISME Journal 7: 592-602.
736 Carritt, D.E. and Carpenter, J.H. 1966. Comparison and evaluation of currently employed
737 modifications of the Winkler method for determining dissolved oxygen in seawater; a
738 NASCO Report. Journal of Marine Research. 24: 286-319.

739 Chance, R., Jickells, T.D., and Baker, A.R. 2015. Atmospheric trace metal concentrations,
740 solubility and deposition fluxes in remote marine air over the south-east Atlantic. Marine
741 Chemistry. Doi: 10.1016/j.marchem.2015.06.028.

742 Conway, T. M., and John, S.G. 2014. The biogeochemical cycling of zinc and zinc isotopes
743 in the North Atlantic Ocean."Global Biogeochemical Cycles. 28: 1111-1128.

744 Coale, K. H. et al. 1996. A massive phytoplankton bloom induced by an ecosystem-scale
745 iron fertilzation experiement in the equatorial Pacific Ocean. Nature. 383: 495-501.

746 Croft, M.T., Lawrence, A.D., Raux-Deery, E., Warren, M.J. and Smith, A.G. 2005. Algae
747 acquire vitamin B_{12} through a symbiotic relationship with bacteria. Nature. 438: 90-93.

748 Croot, P.L., and Heller, M.I., 2012. The importance of kinetics and redox in the
749 biogeochemical cycling of iron in the surface ocean. Frontiers in Microbiology, 3. Doi:
750 10.3389/fmicb.2012.00219.

751 Croot, P.L., Streu, P., Baker, A.R., 2004. Short residence time for iron in surface seawater
752 impacted by atmospheric dry deposition from Saharan dust events. Geophysical Research
753 Letters, 31. Doi: 10.1029/2004gl020153.

754 Cruz-López, R., and Maske, H. 2016. The vitamin B_1 and B_{12} required by themMarine
755 dinoflagellate *Lingulodinium polyedrum* can be provided by its associated bacterial
756 community in culture."Frontiers in Microbiology 7. DOI: 10.3389/fmicb.2016.00560.

757 de Baar, H. J. W. et al. 2008. Titan: A new facility for ultraclean sampling of trace elements
758 and isotopes in the deep oceans in the international GEOTRACES program. Marine
759 Chemistry. 111: 4-21.

760 Doherty, O. M., Riemer, N., and Hameed, S. 2012. Control of Saharan mineral dust transport
761 to Barbados in winter by the Intertropical Convergence Zone over West Africa. J.
762 Geophysical Research Atmosphere. 117. DOI: 10.1029/2012JD017767.

763

764 Doherty, O.M., Riemer, N., and Hameed, S., 2014. Role of the convergence zone over West
765 Africa in controlling Saharan mineral dust load and transport in the boreal summer. Tellus B,
766 66. Doi: 10.3402/tellusb.v66.23191.

767 Donat, J.R., and Bruland, K.W. 1988. Direct determination of dissolved cobalt and nickel in
768 seawater by differential pulse cathodic stripping voltammetry preceded by adsorptive
769 collection of cyclohexane-1,2-dione dioxime complexes. Analytical Chemistry. 60: 240-244.

770 Duce, R. A., et al. 1991. The atmospheric input of trace species to the world ocean. Global
771 Biogeochemical Cycles. 5, 193-259.

772 Duce, R.A., and Tindale, N.W. 1991. Atmospheric transport of iron and its deposition to the
773 ocean. Limnology and Oceanography. 36: 1715-1736.

774 Dulaquais, G. et al. 2014a. Contrasting biogeochemical cycles of cobalt in the surface
775 western Atlantic Ocean. Global Biogeochemical Cycles. 28. Doi: 10.1002/2014GB004903.

776 Dulaquais, G., Boye, M., Rijkenberg, M.J.A., and Carton, X. 2014b. Physical and
777 remineralization processes govern the cobalt distribution in the deep western Atlantic Ocean.
778 Biogeosciences. 11: 1561-1580.

779 Durand, M.D., Olson, R.J., and Chisholm, S.W. 2001. Phytoplankton population dynamics at
780 the Bermuda Atlantic time-series station in the Sargasso Sea. Deep Sea Research II. 48:
781 1983-2003.

782 Ellwood, M. J., and van den Berg, C.M.G. 2001. Determination of organic complexation of
783 cobalt in seawater by cathodic stripping voltammetry."Marine Chemistry. 75: 33-47.

784 Evangelista, H. et al. 2010. Inferring episodic atmospheric iron fluxes in the western South
785 Atlantic. Atmospheric Environment. 44: 703-712.

786 Fitzsimmons, J. N., Zhang, R., and Boyle, E.A. 2013. Dissolved iron in the tropical North
787 Atlantic Ocean. Marine Chemistry. 154: 87-99.

788 Gong, N., Chen, C., Xie, L., Chen, H., Lin, X., and Zhang, R. 2005. Characterization of a
789 thermostable alkaline phosphatase from a novel species *Thermus yunnanensis sp. nov.* and
790 investigation of its cobalt activation at high temperature. Biochimica Biophysica Acta. 1750:
791 103-111.

792 Grashoff, K., Erhardt, M., and Kremling, K. 1983. Methods in Seawater Analyses. Weinheim:
793 Verlag Chemie.

794 Hartmann, M., Gomez-Pereira, P., Grob, C., Ostrowski, M., Scanlan, D.J., and Zubkov, M.V.
795 2014. Efficient CO_2 fixation by surface *Prochlorococcus* in the Atlantic Ocean. ISME J 8:
796 2280-2289.

797 Hastenrath, S., and Merle, J. 1987. Annual cycle of subsurface thermal structure in the
798 tropical Atlantic Ocean. Journal of Pysical Oceanography. 17: 1518-1538.

799 Hatta, M., Measures, C.I., Wu, J., Roshan, S., Fitzsimmons, J.N., Sedwick, P., and, Morton,
800 P., 2014. An overview of dissolved Fe and Mn Distributions during the 2010–2011 U.S.
801 GEOTRACES north Atlantic Cruises: GEOTRACES GA03. Deep Sea Research Part II.
802 116:117-129.

803 Heller, M.I., Gaiero, D. M., and Croot, P. L., 2013. Basin scale survey of marine humic
804 fluorescence in the Atlantic: Relationship to iron solubility and H_2O_2. Global Biogeochemical
805 Cycles, 27, 88-100.

806 Helliwell, K.E., Lawrence, A.D., Holzer, A., Kudahl, U.J., Sasso, S., Krautler, B., Scanlan,
807 D.J., Warren, M.J., and Smith A.G. 2016. Cyanobacteria and eukaryotic algae use different
808 chemical variants of vitamin B_{12}. Current Biology 26: 999-1008.

809 Helmers, E., and Schrems, O.1995. Wet deposition of metals to the tropical North and the
810 South Atlantic Ocean. Atmospheric Environment. 29: 2475-2484.

811 Heywood, J.L., Zubkov, M.V., Tarran, G.A., Fuchs, B.M., and Holligan, P.M. 2006.
812 Prokaryoplankton standing stocks in oligotrophic gyre and equatorial provinces of the
813 Atlantic Ocean: Evaluation of inter-annual variability. Deep Sea Research Part II. 53: 1530-
814 1547.

815 Ji, Y., and Sherrell, R.M. 2008. Differential effects of phosphorus limitation on cellular metals
816 in Chlorella and Microcystis. Limnology and Oceanography 53: 1790-1804.

817 Jickells, T.D., et al. 2005. Global iron connections between desert dust, ocean
818 biogeochemistry and climate. Science. 308: 67-71.

819 Johnson, K. S., Gordon, R. M. and Coale, K. H. 1997. What controls dissolved iron
820 concentrations in the world ocean? Marine Chemistry. 57: 137-161.

821 Jullion, L., Heywood, K.J. Naveira Garabato, A C. and Stevens, D.P. 2010. Circulation and
822 water mass modification in the Brazil-Malvinas Confluence. Journal of Physical
823 Oceanography. 40: 845–864.

824 Karstensen, J., Stramma, L. and Visbeck, M. 2008. Oxygen minimum zones in the eastern
825 tropical Atlantic and Pacific Oceans. Progress in Oceanography. 77: 331-350.

826 Kathuria, S., and Martiny, A.C., 2011. Prevalence of a calcium-based alkaline phosphatase
827 associated with the marine cyanobacterium Prochlorococcus and other ocean bacteria.
828 Environmental Microbiology, 13, 74-83.

829 Knauer, G.A., Martin, J.H. and Gordon, R.M. 1982. Cobalt in north-east Pacific waters.
830 Nature. 297: 49-51.

831 Kaufman, Y. J., Koren, I., Remer., L.A., Tanré, D., Ginoux, P., and Fan, S. 2005. Dust
832 transport and deposition observed from the Terra-Moderate Resolution Imaging
833 Spectroradiometer (MODIS) spacecraft over the Atlantic Ocean. Journal of Geophysical
834 Research. 110. Doi:10.1029/2003JD004436

835 Kim, G., and, Church, T.M., 2002. Wet deposition of trace elements and radon daughter
836 systematics in the South and equatorial Atlantic atmosphere. Global Biogeochem. Cycles,
837 16. Doi: 10.1029/2001gb001407.
838 Küpper, H. et al. 2008. Iron limitation in the marine cyanobacterium Trichodesmium reveals
839 new insights into regulation of photosynthesis and nitrogen fixation. New Phytologist 179:
840 784-798.
841 Laes, A. et al. 2007. Sources and transport of dissolved iron and manganese along the
842 continental margin of the Bay of Biscay. Biogeosciences. 4: 181-194.
843 Liu, X., and Millero, F.J., 2002. The solubility of iron in seawater. Marine Chemistry, 77, 43-
844 54.

845 Lohan, M. C., Aguilar-Islas, A. M., Franks, R. P. and Bruland, K. W. 2005. Determination of
846 iron and copper in seawater at pH 1.7 with a new commercially available chelating resin,
847 NTA Superflow. Analytica Chimica Acta. 530: 121-129.

848 Longhurst, A. 1998. Ecological Geography of the Sea. San Diego: Academic Press.

849 Mackey, K. R. M., Chien, C.-T., Post, A.F., Saito, M.A., and Paytan, A. 2015. Rapid and
850 gradual modes of aerosol trace metal dissolution in seawater. Frontiers in Microbiology. 5: 1-
851 11.

852 Mahaffey, C., Reynolds, S., Davis, C.E., and Lohan, M.C. 2014. Alkaline phosphatase
853 activity in the subtropical ocean: insights from nutrient, dust and trace metal addition
854 experiments. Frontiers in Marine Science. 1. Doi: 10.3389/fmars.2014.00073.

855 Mahowald, N. et al. 1999. Dust sources and deposition during the last glacial maximum and
856 current climate: a comparison of model results with paleodata from ice cores and marine
857 sediments. Journal of Geophysical Research. 104:15895–916.

858 Martin, J. H. and Gordon, R.M. 1988. Northeast Pacific iron distributions in relation to
859 phytoplankton productivity. . Deep-Sea Research. 35: 177-196.

860 Martin, J. H. 1990. Glacial-interglacial CO_2 change: the iron hypothesis. Paleoceanography.
861 5: 1-13.

862 Mather, R. L. et al. 2008. Phosphorus cycling in the North and South Atlantic Ocean
863 subtropical gyres. Nature Geoscience 1: 439-443.

864 Mawji, E., Gledhill, M., Milton, J.A., Tarran, G.A., Ussher, S., Thompson, A., Wolff, G.A.,
865 Worsfold, P.J., and Achterberg, E.P., 2008. Hydroxamate Siderophores: Occurrence and
866 Importance in the Atlantic Ocean. Environmental Science & Technology, 42, 8675-8680.

867 Measures, C.I., Landing, W.M., Brown, M.T. and Buck, C.S. 2008. High-resolution Al and Fe
868 data from the Atlantic Ocean CLIVAR-CO_2 repeat hydrography A16N transect: extensive

869 linkages between dust and upper ocean geochemistry. Global Biogeochemical Cycles. 22.
870 Doi: 10.1029/2007GB003042.

871 Mémery, L. et al. 2000. The water masses along the western boundary of the south and
872 equatorial Atlantic. Progress in Oceanography. 47: 69-98.

873 Millero, F., Yao, W., and Aicher, J. 1995. The speciation of Fe(II) and Fe(III) in natural
874 waters. Marine Chemistry. 50: 21-39.

875 Moffett, J.W., and Ho, J. 1996. Oxidation of cobalt and manganese in seawater via a
876 common microbially catalyzed pathway. Geochimica et Cosmochimica Acta. 60: 3415-3424.

877 Moore, C. M. et al. 2013. Processes and patterns of oceanic nutrient limitation. Nature
878 Geoscience. 6: 701-710.

879 Moore, C.M., Mills, M.M., Milne, A., Langlois, R., Achterberg, E.P., Lochte, K., Geider, R.J.,
880 and La Roche, J., 2006. Iron limits primary productivity during spring bloom development in
881 the central North Atlantic. Global Change Biology. 12,, 626-634.

882 Moore, J. K., Doney, S. C., Glover, D. M. and Fung, I. Y. 2002. Iron cycling and nutrient-
883 limitation patterns in surface waters of the World Ocean.Deep Sea Research: Part II: Topical
884 Studies in Oceanography. 49: 463-507.

885 Morel, F. M. M., Reinfelder, J.R., Roberts, S.B., Chamberlain, C.P., Lee, J.G. and Yee, D.
886 1994. Zinc and carbon co-limitation of marine phytoplankton. Nature. 369: 740-742.

887 Morel, F. M. M. and Price, N.M. 2003. The biogeochemical cycles of trace metals in the
888 oceans. Science. 300: 944-947.

889 Nielsdottir, M. C., Moore, C.M., Sanders, R., Hinz, D.J., and Achterberg, E.P. 2009. Iron
890 limitation of the post bloom phytoplankton communities in the Iceland Basin. Global
891 Biogeochemical Cycles. 23. Doi: 10.1029/2008GB003410.

892 Noble, A.E., Saito, M.A., Maiti, K. and Benitez-Nelson, C., 2008. Cobalt, manganese, and
893 iron near the Hawaiian Islands: a potential concentrating mechanism for cobalt within a
894 cyclonic eddy and implications for the hybrid-type trace metals. Deep Sea Research. Part II.
895 55: 1473-1490.

896 Noble, A. E. et al. 2012. Basin-scale inputs of cobalt, iron, and manganese from the
897 Benguela-Angola front to the South Atlantic Ocean. Limnology and Oceanography. 57: 989-
898 1010.

899 Obata, H., Karatani, H. and Nakayama, E. 1993. Automated determination of iron in
900 seawater by chelating resin concentration and chemiluminescence detection. Analytical
901 Chemistry. 65: 1524-1528.

902 Pohl, C., Croot, P. L., Hennings, U., Daberkow, T., Budeus, G. and Rutgers van der Loeff,
903 M. 2010. Synoptic transects on the distribution of trace elements (Hg, Pb, Cd, Cu, Ni, Zn,
904 Co, Mn, Fe, and Al) in surface waters of the Northern and Southern East Atlantic. Journal of
905 Marine Systems. 84: 24-41.

906 Powell, C.F., Baker, A.R., Jickells, T.D., Bange, H.W., Chance, R.J., Yodle, C., , 2015.
907 Estimation of the atmospheric flux of nutrients and trace metals to the eastern tropical North
908 Atlantic Ocean. Journal of the Atmospheric Sciences, 4029-4045.

909 Prospero, J. M., and Carlson, T.N. 1972. Vertical and areal distribution of Saharan dust over
910 the Equatorial North Atlantic Ocean. Journal of Geophysical Research. 77: 5255-5265.

911 Prospero, J. M., Ginoux, P., Torres, O., Nicholson, S.E. and Thomas, T.E. 2002.
912 Environmental characterization of global sources of atmospheric dust identified with the
913 Nimbus 7 Total Ozone Mapping Spectrometer (TOMS) absorbing aerosol product. Reviews
914 of Geophysics. 40. Doi: 10.1029/2000RG000095.

915 Richier, S., Macey, A.I., Pratt, N.J., Honey, D.J., Moore, C.M., and Bibby, T,S., 2012.
916 Abundances of iron-binding photosynthetic and nitrogen-fixing proteins of Trichodesmium

both in culture and in situ from the North Atlantic. PLoS ONE, 7. Doi: 10.1371/journal.pone.0035571.

Ridame, C., Moutin, T., and Guieu, C., 2003. Does phosphate adsorption onto Saharan dust explain the unusual N/P ratio in the Mediterranean Sea? Oceanologica Acta, 26, 629-634.

Rijkenberg, M.J.A., Middag, R., Laan, P., Gerringa, L.J.A., van Aken, H.M., Schoemann, V., de Jong, J.T.M., and de Baar, H.J.W., 2014. The distribution of dissolved iron in the West Atlantic Ocean. PLoS ONE, 9. Doi: 10.1371/journal.pone.0101323.

Rijkenberg, M.J.A., Steigenberger, S., Powell, C.F., van Haren, H., Patey, M.D., Baker, A.R., and Achterberg, E.P., 2012. Fluxes and distribution of dissolved iron in the eastern (sub-) tropical North Atlantic Ocean. Global Biogeochemical Cycles. 26. Doi: 10.1029/2011gb004264.

Robinson, C. 2006. The Atlantic Meridional Transect (AMT) Programme: A contextual view 1995-2005. Deep Sea Research. Part II: Topical Studies in Oceanography. 53: 1485-1515.

Rodriguez, I.B., and Ho,T.-Y. 2015. Influence of Co and B_{12} on the growth and nitrogen fixation of *Trichodesmium*. Frontiers in Microbiology 6. Doi: 10.3389/fmicb.2015.00623.

Roshan, S., and Wu, J. 2015. Water mass mixing: The dominant control on the zinc distribution in the North Atlantic Ocean. Global Biogeochemical Cycles. 29: 1060-1074.

Rubin, M., Berman-Frank, I., Shaked, Y. 2011. Dust-and mineral-iron utilization by the marine dinitrogen-fixer *Trichodesmium*. Nature Geoscience, 4:529-534.

Rudnick, R.L., and Gao, S., 2003. Composition of the continental crust. In H.D. Holland, and Turekian, K.K. (Ed.), Treatise on Geochemistry (pp. 1-64). Oxford: Elsevier.

Rue, E. L., and Bruland, K.W. 1995. Complexation of iron (III) by natural organic ligands in the Central North Pacific as determined by a new competiative ligand equilibrium/ adsorptive cathodic stripping voltammetric method. Marine Chemistry. 50: 117-138.

941 Saito, M. A. and Goepfert, T. J. 2008. Zinc-cobalt colimitation of *Phaeocystis antarctica*.
942 Limnology and Oceanography. 53: 266-275.

943 Saito, M. A., Goepfert, T.J., Ritt, J.T. 2008. Some thoughts on the concept of colimitation:
944 Three definitions and the importance of bioavailability. Limnology and Oceanography. 53:
945 276-290.

946 Saito, M. A., and Moffett, J.W. 2001. Complexation of cobalt by natural organic ligands in the
947 Sargasso Sea as determined by a new high-sensitivity electrochemical cobalt speciation
948 method suitable for open ocean work. Marine Chemistry. 75: 49-68.

949 Saito, M.A., and Moffett, J.W. 2002. Temporal and spatial variability of cobalt in the Atlantic
950 Ocean. Geochimica et Cosmochimica Acta. 66, 1943-1953.

951 Saito, M.A., Moffett, J.W., Chisholm, S. and Waterbury, J.B. 2002. Cobalt limitation and
952 uptake in *Prochlorococcus*. Limnology and Oceanography .47: 1629-1636.

953 Saito, M.A., Rocap, G. and Moffett J.W. 2005. Production of cobalt binding ligands in a
954 *Synechococcus* feature at the Costa Rica upwelling dome. Limnology and Oceanography.
955 50: 279-290.

956 Sanudo-Wilhelmy, S.A., Kustka, A.B., Gobler, C.J., Hutchins, D.A., Yang, M., Lwiza, K.,
957 Burns, J., Capone, D.G., Raven, J.A., Carpenter, E.J., 2001. Phosphorus limitation of
958 nitrogen fixation by *Trichodesmium* in the central Atlantic Ocean. Nature, 411, 66-69.

959 Sarthou, G. et al. 2003. Atmospheric iron deposition and sea-surface dissolved iron
960 concentrations in the eastern Atlantic Ocean. Deep Sea Research. Part I: Oceanographic
961 Research Papers. 50: 1339-1352.

962 Sarthou, G. et al. 2007. Influence of atmospheric inputs on the iron distribution in the
963 subtropical North-East Atlantic Ocean. Marine Chemistry. 104: 186-202.

964 Schlosser, C. et al. 2013. Seasonal ITCZ migration dynamically controls the location of the
965 (sub)tropical Atlantic biogeochemical divide. Proceedings of the National Academy of
966 Sciences. Doi: 10.1073/pnas.1318670111.

967 Shaked, Y., and Lis, H., 2012. Dissassembling iron availability to phytoplankton. Frontiers in
968 Microbiology, 3. Doi: 10.3389/fmicb.2012.00123.

969 Shelley, R. U., Morton, P.L., and Landing, W.M. 2015. Elemental ratios and enrichment
970 factors in aerosols from the US-GEOTRACES North Atlantic transects. Deep Sea Research.
971 Part II: Topical Studies in Oceanography. 116: 262-272.

972 Shelley, R. U. et al. 2012. Controls on dissolved cobalt in surface waters of the Sargasso
973 Sea: Comparisons with iron and aluminum. Global Biogeochemical. Cycles. 26. Doi:
974 10.1029/2011gb004155.

975 Shelley, R. U., Zachhuber, B. Sedwick, P.J., Worsfold, P.J. and Lohan, M.C. 2010.
976 Determination of total dissolved cobalt in UV-irradiated seawater using flow injection with
977 chemiluminescence detection. Limnology and. Oceanography: Methods. 8: 352-362.

978 Sholkovitz, E.R., and Copland, D. 1981. The coagulation, solubility and adsorption properties
979 of Fe, Mn, Cu, Ni, Cd, Co and humic acids in a river water. Geochimica et Cosmochimica
980 Acta. 45: 181-189.

981 Sultan, B., and Janicot, S. 2000. Abrupt shift of the ITCZ over West Africa and intra-seasonal
982 variability. Geophysical Research Letters. 27: 3353-3356.

983 Sunda, W.G. and Huntsman, S.A. 1995a. Cobalt and zinc inter-replacement in marine
984 phytoplankton: biological and geochemical implications. Limnology and Oceanography. 40:
985 1404-1417.

986 Sunda, W. G., and Huntsman, S.A.1995b. Iron uptake and growth limitation in oceanic and
987 coastal phytoplankton. Marine Chemistry. 50: 189-206.

988 Tarran, G.A., Heywood, J.L. and Zubkov, M.V. 2006. Latitudinal changes in the standing
989 stocks of nano- and picoeukaryotic phytoplankton in the Atlantic Ocean. Deep Sea
990 Research. Part II. 53: 1516-1529.

991 Thuroczy, C.-E., Boye, M., and Losno, R., 2010. Dissolution of cobalt and zinc from natural
992 and anthropogenic dusts in seawater. Biogeosciences, 7, 1927-1936.

993 Timmermans, K.R., Snoek, J., Gerringa, L.J.A., Zondervan, I., de Baar, H.J.W. 2001. Not all
994 eukaryotic algae can replace zinc with cobalt: *Chaetoceros calcitrans* (Bacillariophyceae)
995 versus *Emiliania huxleyi* (Prymnesiophyceae). Limnology and Oceanography. 46: 699-703.

996 Tsamalis, C., Chédin, A., Pelon, J., and Capelle, V., 2013. The seasonal vertical distribution
997 of the Saharan Air Layer and its modulation by the wind. Atmospheric. Chemistry and.
998 Physics, 13, 11235-11257.

999 Tyrrell, T., Maranon, E., Poulton, A.J., Bowie, A.R., Harbour, D.S., and Woodward, E.M.S.,
1000 2003. Large-scale latitudinal distribution of Trichodesmium spp. in the Atlantic Ocean.
1001 Journal of Plankton Research., 25, 405-416.

1002 Ussher, S.J. et al. 2013. Impact of atmospheric deposition on the contrasting iron
1003 biogeochemistry of the North and South Atlantic Ocean. Global Biogeochemical Cycles. 27:
1004 1096-1107. Doi: 10.1002/gbc.20056.

1005 Ussher, S. J. et al. 2007. Distribution and redox speciation of dissolved iron on the European
1006 continental margin. Limnology and Oceanography. 52: 2530-2539.

1007 van den Berg, C. M. G. 1995. Evidence for organic complexation of iron in seawater. Marine
1008 Chemistry. 50: 139-157.

1009 Vega, M. and.van den Berg, C.M.G. 1997. Determination of cobalt in seawater by catalytic
1010 adsorptive cathodic stripping voltammetry. Analytical Chemistry. 69: 874-881.

1011 Welschmeyer, N.A., 1994. Fluorometric Analysis of chlorophyll a in the presence of
1012 chlorophyll b and pheopigments. Limnology and Oceanography. 39: 1985-1992.

1013 Westrich, J. R., Ebling, A.M., Landing, W.M., Joyner, J.L., Kemp, K.M., Griffin, D.W., and
1014 Lipp, E.K. 2016. Saharan dust nutrients promote Vibrio bloom formation in marine surface
1015 waters. PNAS 113: 5964-5969.

1016 Wong, G.T.F., Pai, S.-C., Chung, S.-W. 1995. Cobalt in the West Philippine Sea.
1017 Oceanologica Acta. 18: 631-638.

1018 Woodward, E.M.S., Rees, A.P. and Stephens, J.A. 1999. The influence of the south-west
1019 monsoon upon the nutrient biogeochemistry of the Arabian Sea. Deep Sea Research: Part
1020 II. 46: 571-591.

1021 Wu, J., Boyle, E. Sunda, W., and Wen, L.-S. 2001. Soluble and colloidal iron in the
1022 oligotrophic North Atlantic and North Pacific. Science. 293: 847-849.

1023 Wu, J., Roshan, S., and Chen, G., 2014. The distribution of dissolved manganese in the
1024 tropical–subtropical North Atlantic during US GEOTRACES 2010 and 2011 cruises. Marine
1025 Chemistry, 166, 9-24.

1026 Wyatt, N. J. et al. 2014. Biogeochemical cycling of dissolved zinc along the GEOTRACES
1027 South Atlantic transect GA10 at 40°S. Global Biogeochemical Cycles. 28: 44-56.

1028